BOLT BERANEK AND NEWMAN INC

CONSULTING • DEVELOPMENT • RESEARCH

TECHNIQUES FOR IMPROVING THE LOW-FREQUENCY PERFORMANCE OF SMALL REVERBERATION CHAMBERS

By Terry D. Scharton, Peter E. Rentz, David Lubman, and Pritchard H. White

Prepared under Contract No. NAS5-21003 by
BOLT BERANEK AND NEWMAN INC.
15808 Wyandotte Street
Van Nuys, California 91406

for

NATIONAL AERONAUTICS AND SPACE ADMINISTRATION

TECHNIQUES FOR IMPROVING THE LOW-FREQUENCY PERFORMANCE OF SMALL REVERBERATION CHAMBERS

By Terry D. Scharton, Peter E. Rentz, David Lubman,
and Pritchard H. White

Prepared under Contract No. NAS5-21003 by
BOLT BERANEK AND NEWMAN INC.
15808 Wyandotte Street
Van Nuys, California 91406

for

NATIONAL AERONAUTICS AND SPACE ADMINISTRATION

TABLE OF CONTENTS

TECHNIQUES FOR IMPROVING THE LOW-FREQUENCY PERFORMANCE OF SMALL REVERBERATION CHAMBERS

By Terry D. Scharton, Peter E. Rentz, David Lubman, and Pritchard H. White
Bolt Beranek and Newman Inc.

INTRODUCTION

This report presents the results of an experimental investigation of the performance characteristics of small reverberation chambers.

In the course of the investigation a small rectangular 135 cubic feet concrete block reverberation chamber was designed, fabricated, and evaluated. The experimental results obtained indicate that the chamber performance evaluated on the basis of statistical reliability and small spatial variations in the time mean-square acoustic pressure is good when the modal overlap index of the chamber is greater than 1/3. In addition to the rectangular chamber configuration, a truncated chamber configuration was experimentally investigated, and the results indicate that the chamber performance is insensitive to the change in the shape of the chamber and again depends only on the modal overlap index, which is a function of the chamber volume and reverberation time.

The primary objective of this investigation was to investigate means of improving the low-frequency performance of small reverberation chambers. The following techniques were investigated: (1) honeycomb panels were placed inside the chamber to enrich the apparent acoustic modal density, (2) absorption was added to increase the modal overlap at low frequencies, (3) feedback devices were used in an attempt to increase the reverberation time, (4) multiple uncorrelated sources were used in an attempt to smooth the frequency and spatial response of the chamber. The addition of the modal enrichment honeycomb panels did increase the apparent acoustic modal density of the chamber and reduce the low-frequency spatial variations. The addition of absorption also resulted in smaller spatial variations in the low-frequency regime. (This technique is currently used to improve the low-frequency response of reverberation rooms used to measure the sound power

radiated by mechanical equipment.) The electronic feedback technique did not work for broad-band noise excitation because of feedback instability at a single frequency in the excitation band. The use of multiple uncorrelated sources did not result in an improvement in the performance obtained with a single source.

In addition an expression is postulated for relating the power delivered by an acoustic driver in a small reverberant room to the power delivered by the driver in a progressive wave tube. This expression is based upon current analytical work and experimental data presented in the literature.

This report describes the design and evaluation of two chamber configurations, discusses the investigation of techniques for improving the low-frequency performance of reverberation chambers, outlines guides for designing reverberation chambers, and presents predictions of the performance of 2135 cubic feet concrete wall and steel wall reverberation chambers.

DESIGN AND EVALUATION OF TWO CHAMBER CONFIGURATIONS

Figure 1 shows the small reverberation chamber used in the experimental portion of this program. The chamber walls are constructed from standard concrete blocks filled with sand, and the ceiling is a steel-reinforced 6 in. concrete slab poured in place. Entrance to the chamber is provided by a 47 in. x 28.5 in. x 2 in. solid core door with a good acoustic seal. The inside of the chamber is finished with a hard smooth plaster.

The inside dimensions of the baseline rectangular chamber configuration are 76.3 in., 62 in., and 49.2 in. which correspond to a volume of 135 ft^3 and a surface area of 160.5 ft^2. The baseline chamber dimensions are approximately in the ratio ($\sqrt[3]{4} : \sqrt[3]{2} : 1$) suggested by Sepmeyer[1/] for good chamber performance.

In order to estimate the performance of a proposed NASA Goddard 2135 ft^3 non-rectangular reverberation chamber, a second chamber configuration shown in Fig. 2, was investigated. The truncated chamber configuration is realized

by inserting a reinforced plasterboard wedge along the lower left side of the chamber. The truncation reduces the chamber floor width from 62 in. to 17 in. and the height of the left chamber wall from 76.3 in. to 32 in. The volume of the truncated chamber is 107 ft^3, and the surface area is 151 ft^2.

Rectangular Chamber

Reverberation time. - Figure 3 shows measurements of the reverberation time of the rectangular chamber shown in Fig. 1 excited with 1/3-octave band noise. In two of the low-frequency 1/3-octave bands, the decay rate traces used to calculate reverberation times showed double slopes. For these frequencies two reverberation times, corresponding to each slope, are plotted in Fig. 3. The measured reverberation times in the low frequency regime from 160 to 500 Hz show considerable scatter but generally range from 3-5 seconds. In the frequency range from 630 to 16,000 Hz, the measured reverberation times decrease in an orderly manner from approximately 3 seconds at 630 Hz to 1/2-second at 16,000 Hz. Also shown in Fig. 3 is an effective absorption coefficient $\bar{\alpha}$ calculated from the reverberation time T according to[2]

$$T = \frac{.049V}{\bar{\alpha}A} \qquad (1)$$

where V is the volume and A the surface area. The effective absorption coefficient ranges from 1% at low frequencies to approximately 5% at 8000 Hz. It should be pointed out that in the high frequency regime the effective absorption coefficient reflects the effect of air absorption as well as the absorption at the walls of the chamber.

Sine sweep response. - Figure 4 shows the sine sweep response of the rectangular chamber. The resonance frequencies f_n of the chamber can be calculated from the characteristic equation given by[3]

$$f_n = \frac{c}{2}\left[\left(\frac{n_x}{L_x}\right)^2 + \left(\frac{n_y}{L_y}\right)^2 + \left(\frac{n_2}{L_2}\right)^2\right]^{1/2}, \qquad (2)$$

where c is the speed of sound in air (1128 ft/sec at 70° F.) and L_x, L_y, and L_z are the room dimensions in feet and the indices n_x, n_y, and n_z take on the values 0, 1, 2, 3, ... etc. The number of modes of the chamber in each one-third octave band has been calculated directly from Eq. 2 using a digital computer program and also from the asymptotic modal density n(f) expression given by[4]

$$n(f) = \frac{4\pi f^2 V}{c^3} + \frac{\pi f A}{2c^2} + \frac{P}{8c} \quad , \qquad (3)$$

where P is the length of chamber wall intersections. The number of modes in each third octave band calculated from Eqs. 2 and 3 are compared in Table I. The results presented in Table I indicate that for the chamber under consideration, the simplified asymptotic modal density expression accurately predicts the number of modes in one-third octave bands.

TABLE I. - COMPARISON OF ASYMPTOTIC AND CHARACTERISTIC EQUATION MODAL DENSITIES FOR 1/3-OCTAVE BANDS

f	n(f)Δf	
	Asymptotic Eq.	Char. Eq.
80	1	1
100	1	1
125	1	2
160	3	3
200	4	3
250	8	7
315	14	16
400	27	25
500	50	48
630	92	93

It is common practice to determine the modal density by counting the number of peaks in the sine sweep response. In Fig. 5 the cumulative resonance frequency distribution, the integral of the modal density, determined from Eq. 3 is compared with a count of the sine sweep peaks exhibited in Fig. 4. The criterion used for counting the sine sweep response peaks was that the peak-to-valley ratio must be 3 dB or more in order that the peak be counted. The results of Fig. 5 indicate that above approximately 315 Hz the response peak count method underestimates the cumulative resonance frequency distribution. The first reason for this is that some of the peaks are missed in the counting procedure in the high frequency regime where the response peaks are closely spaced in frequency. This difficulty can be alleviated by measuring the sine sweep response with a linear frequency sweep to increase the frequency resolution. The second reason lies in the fact that in the high frequency regime, where many response modes occur within the band width of a single mode (the region of modal overlap), the response peaks do not in fact even correspond to modal resonance frequencies.[5]

Modal overlap. - The index of modal overlap, M, provides a measure of the lowest usable frequency in a well designed reverberation room. The index M is defined as the product of the 3 dB bandwidth Δ of a typical modal resonance and the modal density n and is thus given by

$$M = \Delta n \quad . \tag{4}$$

The 3 dB bandwidth of a modal resonance is given by

$$\Delta = \frac{2.2}{T} \quad , \tag{5}$$

where T is the reverberation time for the mode in question. Using the first term of the asymptotic formula for modal density (Eq. 3) in Eqs. 4 and 5 yields for the frequency f_c corresponding to a modal overlap index M

$$f_c = \left[\frac{M\, c^3 T}{8.8\pi V}\right]^{1/2} \quad . \tag{6}$$

Equation 6 may be used to find the cutoff frequency f_c for statistical behavior of a well designed reverberation room with known volume and reverberation time. Alternatively, it may be used to find the required size for a reverberation room intended to operate at frequencies as low as f_c.

In either case one has first to select a minimum value of M. The appropriate value of M is an important (an open) question. The current practice is to choose M = 3, however, the results of this study indicate that this choice may be too conservative. In other words, a well designed room may be useful to lower frequencies than is given by Eq. 6 with M = 3. The question of picking the appropriate value of modal overlap index is considered further in the next section.

Spatial variations. - Figure 6 presents measured and predicted spatial variations in the rectangular chamber. Figure 6 also presents the value of modal overlap as a function of frequency calculated from Eq. 6 using the measured values of reverberation time reported in Fig. 3.

The empirical values of the standard deviation of sound pressure level, S, are computed from a set of 60 sound pressure levels measured at various locations in the chamber with 1/10-octave band and 1/3-octave band noise excitation. The locations were chosen for experimental convenience to lie on the curved surface of an imaginary cylinder 2 ft in diameter and 4 ft long. The cylinder axis is normal to the chamber floor and passes through the center of the chamber. All measurement locations were at least 1 ft from the chamber boundaries. S is computed from the set of 60 measurement levels, $[L_i]$, using the customary formula for the standard deviation of a group of measurements given by

$$S^2 = \frac{n \sum_{i=1}^{n} L_i^2 - \left(\sum_{i=1}^{n} L_i \right)^2}{n(n-1)} \quad . \qquad (7)$$

Expressed in this way, S is an index of the magnitude of spatial variation in the chamber. It is independent of the mean level, meaning S would not change if the experiment were repeated at a different sound pressure level, and it is independent of time because the individual sample levels are already time-averaged quantities.

The predicted standard deviation in dB units, σ, which applies only at the high frequencies where M is greater than 1 is given by[6]

$$\sigma = 5.6(1 + 0.23\ BT)^{-1/2} \quad , \qquad (8)$$

where B is the equivalent flat spectrum bandwidth of the excitation. (B = 0.23 f_o for 1/3-octave bands and B = 0.11 f_o for 1/10-octave bands, where f_o is the band center frequency.)

The data presented in Fig. 6 indicate that the predicted and empirical values of spatial variation for 1/10 and 1/3 octave band excitation are in essential agreement at frequencies above 1000 Hz corresponding to modal overlap indexes greater than 1. However the measured values of spatial variation do not exceed 1 dB until one goes to frequencies less than 630 Hz. (Notice that the measured spatial variations for 1/10-octave band excitation change slope considerably at 630 Hz.) The data presented in Fig. 6 thus indicate that the rectangular chamber is useful at frequencies above 630 Hz or at modal overlap indices above 1/3.

The measured reverberation times presented in Fig. 3 also lend credence to the choice of lower cutoff frequency of 630 Hz and modal overlap index of 1/3. At frequencies below 630 Hz the reverberation decay measurements exhibit irregularities of various kinds such as double slopes and fluctuation in the mean reverberation time from frequency band to band. At frequencies above 630 Hz the decay curves show single slopes and a systematic trend in the mean slope from frequency band to band.

Truncated Chamber

Reverberation time. - Figure 7 shows 1/3-octave band excitation measurements of the reverberation time of the truncated chamber. The measured reverberation times have also been converted into an effective absorption coefficient using Eq. 1. The measured reverberation times show considerable scatter and are sometimes multivalued at frequencies below approximately 400 Hz and decrease monotonically with increasing frequency above 400 Hz. Comparison of the calculated absorption coefficients for the truncated chamber (Fig. 7) and the rectangular chamber (Fig. 3) indicates that the effective absorption coefficient of the two configurations are approximately the same at all frequencies. The reverberation time of the truncated chamber is approximately 85% of the reverberation time of the rectangular chamber in accordance with the dependency of the reverberation time upon the volume to area ratio of the two chambers (see Eq. 1).

Sine sweep response. - The sine sweep response of the truncated chamber is shown in Fig. 8. Comparison of the sine sweep response of the truncated chamber (Fig. 8) with the sine sweep response of the rectangular chamber (Fig. 4) indicates that the truncated shape did not result in excessive frequency irregularity or bunching of the chamber resonant frequencies. Therefore it may be concluded that the asymptotic modal density expression given by Eq. 3 applies equally well to the truncated or rectangular chamber if the appropriate volume, surface area, and intersection length are used.

Spatial variations. - The measured and predicted spatial variations for 1/10-octave and 1/3-octave band noise excitation are shown in Fig. 9 for the truncated chamber. The measured spatial variations in both one-tenth and one-third octave bands are slightly larger in the truncated chamber than in the rectangular chamber. In the high modal overlap regime where Eq. 8 applies, the higher spatial variation results from the decreased reverberation time of the truncated chamber. In the region of low modal overlap, M < 1, it has been shown that the spatial variation is inversely proportional to the chamber modal density.[1] The larger variations of the truncated chamber in the low frequency regime result because the truncated chamber has slightly less volume and therefore, a smaller modal density than the rectangular chamber configuration. The spatial variation data presented in Fig. 9 indicate a change of slope in the frequency range of 500 or 630 Hz, which as in the case with the rectangular chamber corresponds to a modal overlap index of approximately one-third.

The data presented in Figs. 3 through 9 indicate that the statistical descriptors: one-third octave band reverberation time, asymptotic modal density, and modal overlap index apply equally well to the truncated and rectangular chamber; and indicate that the difference in the shape of the chambers does not significantly affect the performance of the truncated chamber. The reverberation time, modal density, and spatial variation data for the two chambers presented in Figs. 3 through 9 all indicate that a modal overlap index of approximately one-third constitutes a reasonable value for calculating the lower cutoff frequency for good statistical performance of the chamber.

TECHNIQUES FOR IMPROVING THE LOW-FREQUENCY PERFORMANCE OF SMALL REVERBERATION CHAMBERS

As indicated in the previous chapter, the performance of a well designed reverberation chamber depends strongly on the modal overlap index M, which is defined as the product of the modal bandwidth and the modal density. In the frequency regime where the modal overlap index is much less than one, the chamber acoustic field is unpredictable and the spatial variations are large; and in the frequency regime where the modal overlap index is of the order unity or larger the chamber acoustic field is well defined in a statistical sense, and the spatial variations in the acoustic field are relatively small. Since the acoustic modal density depends primarily on the chamber volume, Eq. 3, it is common practice to design very large reverberation chambers in order to obtain a high value of modal overlap index and hence good performance in the low-frequency regime.

If it were possible to overcome the low-frequency problem, a small reverberant acoustic chamber would in many cases offer advantages over a large chamber. The most obvious advantage is cost reduction. In a case where the test item is a relatively small spacecraft or aerospace component, the costs associated with constructing a large chamber and procuring the acoustic drivers required to achieve the specified acoustic levels in a large chamber can be sufficiently greater than the cost associated with doing the job in a small chamber. A small chamber also offers the advantage that it may be converted to a direct field acoustic test facility by adding absorption.

This section describes an investigation of several techniques for improving the low-frequency performance of small reverberation chambers. The first technique involves the addition of flexible honeycomb panels to the chamber in order to increase the apparent acoustic modal density and, thereby the modal overlap index, at low frequencies.

The second technique consists of adding absorption to decrease the reverberation time and thereby increase the modal bandwidth and modal overlap index at low frequencies. This technique is not quite as appealing as the idea of increasing modal density because decreasing reverberation

time carries with it the penalty of increasing the high-frequency spatial variation (see Eq. 8) and also the penalty of increasing the amount of sound power required to generate a given sound pressure level in the chamber. The third technique for improving the low-frequency performance involves the use of electronic feedback devices to artificially increase the reverberation time in the chamber, and the fourth technique involves the use of uncorrelated drivers to increase the spatial uniformity of the response.

Modal Enrichment Panels

In order for modal enrichment panels to be effective, it is necessary that the panels couple strongly to the acoustic field and also exhibit a high modal density at low frequencies. The requirement that the panels couple strongly to the acoustic field may be expressed analytically by requiring that the time average energy in a panel vibration mode θ_p be approximately equal to the time average energy in the acoustical mode θ_a which drives the panel. This requirement is[8]

$$\frac{\theta_p}{\theta_a} = \frac{\eta_{rad}}{\eta_{rad} + \eta_{int}} \approx 1 \qquad (9)$$

where η_{rad} indicates the radiation loss factor of the panel and η_{int} indicates the internal loss factor of the panel. Thus for strong coupling, the radiation loss factor must be of the same order of magnitude as the internal loss factor.

The radiation loss factor of a panel is[9]

$$\eta_{rad} = \frac{\rho c \sigma}{2\pi f \rho_s} \qquad (10)$$

where ρc is the characteristic acoustic impedance, ρ_s is the panel mass per unit area, and σ is the radiation efficiency which depends primarily on the coincidence frequency of the panel and, in the low-frequency regime, on the panel boundary conditions. Thus in order for the panel to be strongly coupled to the acoustic field at low frequencies, the panel must have light surface weight, a low coincidence frequency, and small internal damping.

To meet these conditions one-half inch thick aluminum honeycomb panels with aluminum cores were chosen. The cross section of a panel is shown in Fig. 10. The face sheets of the panels are 1/100 in. thick, the honeycomb core consists of 3/8 in. cells of one mill thickness, and the combined weight of the surface panels, core, and adhesive is 0.43 lb/ft^2. Four panels are suspended approximately 6 in. from the four walls, one panel is suspended 6 in. from the ceiling, and one panel is supported on rubber foam approximately 6 in. off the floor as shown in Fig. 10. The total surface area of the panels, counting one side, is approximately 90 ft^2.

The predicted radiation loss factor η_{rad} of a free-free unbaffled honeycomb panel as calculated from Eq. 10 is shown in Fig. 11. Also shown in Fig. 11 is the measured total loss factor of the panels ($\eta_{total} = \eta_{rad} + \eta_{int}$). The total loss factor of a panel was measured by suspending a panel in an anechoic chamber, exciting the panel with a shaker excited with an octave band of noise, and measuring the decay rate of the panel vibration when the excitation is terminated. Comparison of the measured total loss factor with the predicted radiation loss factor indicates that the predicted radiation loss factor is too large in the mid-frequency range. The explanation for this discrepancy may lie in the fact that the simple bending wave theory used to calculate the radiation efficiency in Eq. 10 does not apply to the thick panel because of shear effects. However the calculation and measurements presented in Fig. 11 indicate that the coupling and internal loss factors of the panel are of the same order of magnitude in the frequency range 200-1000 Hz and therefore the panels should be strongly coupled to the reverberant chamber acoustic field in this frequency regime.

The second requirement for enriching the modal density is that the panels have a high modal density compared to the acoustic modal density in the frequency range of interest. The bending modal density of a panel is[10]

$$n(f) = \frac{S}{2\kappa C_\ell} \qquad (11)$$

where κ is the radius of gyration, C_ℓ is the speed of longitudinal waves, and S is the total surface area of the panels. The panel modal density calculated according

to Eq. 11 with S = 90 sq ft, κ = 1/4 in., and C_ℓ = 17,000 ft/sec is shown in Fig. 12 along with the rectangular chamber acoustic modal density calculated according to the first term of Eq. 3. The panel modal density is equal to the acoustic modal density at a frequency of approximately 225 Hz. Therefore we may anticipate that at a frequency of approximately 225 Hz the addition of honeycomb panels should approximately double the apparent modal density of the reverberation chamber.

Unfortunately the requirement that the panels couple strongly to the acoustic field at low frequencies is somewhat in contradiction to the requirement that the panels have high modal density at low frequencies, since the requirement for strong coupling requires thick panels in order to achieve a low coincidence frequency and the requirement for high modal density requires thin flexible panels. Ideally it would have been advantageous to enrich the modal density of the honeycomb panels by the addition of secondary structure using a technique that has been previously investigated.[11-13] The results of this previous research indicate that it would be possible to increase the modal density of the honeycomb panels by as much as a factor of 10 which would extend the frequency range of acoustic modal enrichment in the present example to a frequency of approximately 1000 Hz. However the enrichment of the honeycomb panel modal density was beyond the scope of the present investigation.

Reverberation time. - The measured reverberation time and calculated absorption coefficient for the rectangular chamber with the modal enrichment panels in place is shown in Fig. 13. The addition of the modal enrichment panels reduced the reverberation times to approximately 50% of the values for the hard-wall-rectangular chamber (see Fig. 3).

Sine sweep response. - Figure 14 shows the sine sweep response of the rectangular chamber with the modal enrichment panels in place. The experimental setup in this experiment was the same as in the sine sweep experiment with the hard-wall rectangular and truncated chamber configurations. The room was excited with a loud-speaker placed in one corner of the room, and the room response was measured with a half-inch microphone placed in the diagonally opposite corner. Comparison of the sine sweep response of the rectangular chamber with the modal enrichment panels with the sine sweep response for the hard-wall

rectangular chamber (Figs. 14 and 4) indicate that the addition of the panels resulted in approximately twice as many peaks in the sine sweep response in the 200 and 250 Hz bands. This is exactly the frequency regime in which one would expect the modal enrichment panels to increase the number of chamber modes, because below 200 Hz the coupling between the panels and the acoustic field is small (Fig. 11) and above 250 Hz the room modal density is larger than the panel modal density (Fig. 12).

Table II shows a comparison of the number of modes in 1/3-octave bands for the hard-wall and honeycomb panel rectangular chambers. Column 2 of Table II lists the number of modes in each 1/3-octave band calculated from the asymptotic equation (Eq.3), column 3 lists the peaks counted in the sine sweep response (Fig. 4) of the hard-wall chamber using a 3 dB criteria, and column 4 presents the peak count for the modally enriched rectangular chamber sine sweep response (Fig. 14). As indicated in Fig. 5, the peak count method does not yield an accurate indication of the modal density for 1/3-octave bands above the 315 Hz band.

TABLE II. - COMPARISON OF HONEYCOMB PANEL AND HARD WALL RECTANGULAR CHAMBER MODAL DENSITIES

	Number of Modes in 1/3-Octave Bands		
1/3-Octave Band Center Frequency	Asymptotic Calculation for Hard-Wall Rectangular Chamber	Peak Count for Hard-Wall Rectangular Chamber	Peak Count for Honeycomb Panel Rectangular Chamber
80	1	1	1
100	1	1	2
125	1	2	2
160	3	2	2
200	4	3	6
250	8	6	12
315	14	10	13
400	27	11	19

Spatial variations. - The predicted and measured spatial variations in the rectangular chamber with modal enrichment panels are presented in Fig. 15 for the cases of 1/10-octave and 1/3-octave band excitation. Comparison of the measured spatial variations presented in Fig. 15 with those presented in Fig. 6 indicates that the addition of the modal enrichment panels significantly decreases the spatial variations in the frequency regime below 630 Hz for both 1/10 and 1/3 octave band excitation. This decrease in spatial variation with the modal enrichment panels in place results from two effects: (1) the increase in the apparent room modal density and (2) the decrease in the reverberation time. The increased absorption experiments described in the next section were conducted in order to isolate these two effects.

Increased Absorption

A small section of fiberglass blanket measuring approximately 2 ft x 1 ft x 1/2 ft was placed in a corner of the hard-wall rectangular chamber in order to increase the absorption without affecting the modal density. The measured reverberation time with 1/3-octave band excitation and the calculated absorption coefficient of the rectangular chamber with the increased absorption is shown in Fig. 16. A comparison of Fig. 16 with Fig. 13 indicates that the reverberation time of the increased absorption configuration is just slightly less than the reverberation time of the modal enrichment configuration.

The measured and predicted spatial variations of the increased absorption chamber are shown in Fig. 17. Comparison of Figs. 17 and Fig. 6 indicates that the addition of absorption decreased the spatial variations in the low-frequency regime below approximately 630 Hz and increased the spatial variations in the high-frequency regime above 630 Hz. To explain this effect notice that the increase in absorption decreases from 630 Hz to 400 Hz the frequency at which the modal overlap index is equal to 1/3. Thus the modal overlap regime in which one expects small spatial variations is extended from 630 Hz down to 400 Hz and the low-frequency spatial variation is thus decreased by the addition of the increased absorption. However in the modal overlap regime above 400 Hz, Eq. 8 indicates that increasing the absorption increases the spatial variations. Thus the addition of absorption raises the spatial variations in the high-frequency regime.

Figure 18 presents the difference in the spatial variations measured with the increased absorption and with the modal enrichment panels for the case of 1/3-octave band excitation. This difference is interpreted as evidence that the decrease in the spatial variations with the modal enrichment panels in place is larger than would be expected on the basis of the panels affecting the reverberation time alone.

Electronic Feedback

A number of experiments were conducted to investigate the possibility of using an active electronic feedback system to artificially increase the reverberation time and modal density of the chamber. The electronic feedback network consisted of a delay line, an artificial reverberation unit, and a power amplifier.

In one configuration the input to the feedback network was provided by a microphone inserted in the chamber and the output was used to drive an auxilliary speaker placed in the chamber. In another configuration the input was provided by an accelerometer mounted on a 1/16 in. x 4 ft x 4 ft aluminum panel suspended in the chamber and the output was again used to drive an auxilliary speaker. In a third configuration the input was provided by an accelerometer mounted on 1/16 in. x 4 ft x 4 ft panel, and the output was used to drive a shaker attached to a second panel. In each case the performance of the chamber evaluated on the basis of reverberation time, sine sweep response, and spatial variations were evaluated using the same speaker excitation and microphone measurement technique employed in the other experiments described in the report.

The electronic feedback experiments utilizing all three configurations proved unsuited to band limited noise excitation. When the gain on the feedback amplifier was turned up sufficiently so that the feedback network would affect the acoustic performance of the chamber, the feedback loop would become unstable and amplify only a particular frequency component in the excitation band. It is hypothesized that the particular frequency component singled out corresponded to a high Q mode of the reverberation chamber. The situation is completely analogous to the feedback phenomena which occurs when the microphone gain in a public address system is turned up too high.

Multiple Uncorrelated Sources

Several experiments were also conducted to investigate the effect of multiple uncorrelated sources on the spatial variations in the chamber response. In the simplest experiment two speakers driven with uncorrelated bands of noise were utilized. The measured spatial variations with the two uncorrelated speakers are shown in Fig. 19. Comparison of the data presented in Fig. 19 with the data presented in Fig. 6 indicates that the use of two uncorrelated speakers did not significantly improve the spatial variations.

Additional experiments were conducted using several small shakers to excite the 1/16 in. x 4 ft x 4 ft panel directly as an alternative to acoustic excitation. In sine sweep experiments with the panel excited mechanically, the acoustic response of the chamber showed many peaks associated with resonances of the panel. However when the panel was driven with small shakers excited with 1/3-octave bands of random noise, the spatial variations in the chamber response did not improve over those associated with the hard wall chamber excited with a single speaker.

DESIGN OF REVERBERATION CHAMBERS

Design Guides

The design of a reverberation chamber involves an iterative procedure to find the optimum solution compatible with several interrelated and often conflicting requirements. The most important descriptors of the performance of a reverberation room are the lower cutoff frequency for good statistical performance, the reverberation time, and the maximum achievable sound pressure level.

The lower cutoff frequency determines the frequency above which the spatial variations in the acoustic field will be relatively small and the test results will be repeatable and consistent in a statistical sense. The lower cutoff frequency also determines the frequency above which the power delivered by an acoustic driver will reach the asymptotic value which the driver would deliver into a progressive wave tube. The reverberation time is an important parameter in determining the lower cutoff frequency, the power required to attain a given sound pressure level in the room, and the high-frequency

spatial variations. The maximum attainable sound pressure level determines how severe a test environment can be realized within a given chamber.

The lower cutoff frequency of a well designed reverberation room is given by Eq. 6 which may be simplified by inserting the speed of sound in air at standard pressure and temperature to yield

$$f_c = 7000[MT/V]^{1/2} \quad . \tag{12}$$

Figure 20 presents a nomograph for evaluating Eq. 12 for either a choice of M = 1/3 or M = 1. The results of this study suggest that the choice M = 1/3 is adequate, however the choice M = 1 is more conservative.

The reverberation time is given by Eq. 1 which is based on an effective absorption coefficient including both the effects of surface absorption and air absorption. This equation may be rewritten in terms of the surface absorption coefficient α and the energy attenuation constant for air m as

$$T = \frac{0.049V}{\alpha A + 4Vm} \quad . \tag{13}$$

The average surface absorption coefficient (the averaging refers to an average over angles of incidence) for very smoothly finished thick concrete walls is approximately 0.01. The average surface absorption coefficient for other types of wall construction is usually a function of frequency and ranges from approximately 0.01 to 0.1 depending primarily on the wall surface weight at low frequencies and the surface finish at high frequencies.[14] The energy absorption coefficient m depends strongly on the relative humidity of the air and m frequency as illustrated in Fig. 22.[15] It is becoming common practice to use nitrogen in lieu of air in reverberation chambers because the energy attenuation constant for nitrogen is significantly smaller than that for air.

The space average sound pressure level (SPL) is related to the sound power level (PWL), the room volume, and the reverberation time by[16,17]

$$SPL = PWL - 10 \log_{10} V + 10 \log T + 19.5 \quad , \tag{14}$$

where the sound pressure level is in decibels referenced to 0.0002 microbar, the sound power level is in decibels referenced to 10^{-13} watts, the room volume is in cubic feet, and the reverberation time is in seconds. Figure 22 presents a nomogram for evaluating Eq. 14.

It has been noted that when the sound power level in Eq. 14 is evaluated on the basis of measurements of the sound power delivered by an acoustic driver into a progressive wave tube, Eq. 14 yields a prediction of the overall sound pressure level in a small reverberation chamber which is approximately 6 decibels higher than measured.[18] For this reason at least one manufacturer of acoustic drivers has recommended a modification of Eq. 14 in which the numerical factor on the right hand side is replaced by 13.5. The apparent contradiction between Eq. 14 and the results based on measured power output into a progressive wave tube can be resolved by hypothesizing that the power output from a high intensity acoustic driver into a small finite room is sometimes much less than the power out of the same driver into a progressive wave termination.

Recent analytical work[19] suggests the following relation between the sound power level delivered to a reverberant room and the sound power level delivered to a progressive wave tube by a high intensity acoustic source

$$PWL)_{\substack{\text{PROGRESSIVE}\\\text{WAVE TUBE}}} - PWL)_{\substack{\text{REVERBERANT}\\\text{ROOM}}} = 10 \log\left(\frac{M+1}{M}\right) , \quad (15)$$

where M is the modal overlap index of the reverberant room. Equation 15 indicates that above the modal overlap frequency ($M > 1$), the power delivered by the driver to the reverberant room will be equal to the power delivered to the progressive wave tube. However, below the modal overlap frequency, Eq. 15 indicates that, assuming reverberation time constant in frequency, the power delivered to a reverberant room will fall off 6 dB per octave as one decreases frequency with respect to that delivered to a progressive wave tube. The analytical result expressed in Eq. 15 is compatible with experimental data.[18]

Figure 23 presents a flow diagram illustrating the iterative procedure necessary to design a reverberant room. The box in the upper left hand corner represents

the low frequency cutoff equation. The inputs to this equation are the modal overlap index criteria, for example M = 1/3, and the lower cutoff frequency. The upper right hand box represents the reverberation time equation. The inputs to this equation are the surface absorption coefficient, which is determined only by the wall construction material, and the energy absorption constant, which is dependent only on the acoustic medium in the chamber. Simultaneous solution of Eqs. 12 and 13 yields unique values for the chamber volume and the reverberation time as a function of frequency. If one is given volume, reverberation time, and a specified available sound power level, the maximum obtainable acoustic level in the chamber may be calculated from Eq. 14.

If the resultant sound pressure level is too low, there are three alternatives: (1) increase the amount of sound power level available, (2) lower the surface absorption coefficient or the energy attenuation constant in order to raise the reverberation time, or (3) settle for a higher value of the cutoff frequency f_c which will in turn decrease the chamber volume and result in higher sound pressure levels.

The spatial variations at frequencies above the cutoff frequency may be determined from Eq. 8 and knowledge of the reverberation time. If the spatial variations are too large, the reverberation time must be increased by lowering the absorption coefficient of the walls or the energy attenuation constant.

This iteration procedure might have to be modified somewhat in a given situation to take into account the initial constraints. For example, in a given situation it might be that the volume of the chamber is fixed by space and cost considerations and the sound pressure level is fixed by test specification. In this case, one would go through the iterative procedure to determine the resultant lower cutoff frequency and the sound power level required to implement the test.

Predicted Performance of a 2,135 Cubic Foot Truncated Chamber

Figures 24 and 25 present the predicted performance of a 2,135 ft^3 truncated chamber. The ratio of the dimensions of the truncated chamber are similar to those of

the small truncated chamber investigated in this study, and the results are used to predict the performance of the 2,135 ft^3 chamber. Two types of wall construction are considered: thick concrete and 1/8 in. steel walls.

Figure 24 presents the predicted 1/3-octave band reverberation times for the concrete wall and steel wall chambers. The predicted reverberation times are based on Eq. 13. The assumed surface absorption coefficient for the concrete walls is assumed to be the same as measured in the model truncated chamber. The concrete walls absorption coefficient varies from .013 in the low frequencies to approximately .03 in the high-frequency regime. The assumed wall absorption coefficient for the 1/8 in. steel walls is taken to be .05 at all frequencies [20/] The reverberation times of the concrete wall chamber are approximately a factor of 4 higher than those of a thin walled steel chamber in the low-frequency regime, and the reverberation times of the two chambers become similar in the high-frequency regime where the effects of air absorption dominate.

Figure 25 presents the predicted spatial variations and the modal overlap index for the concrete and steel wall configurations. The spatial variations in the high-frequency regime are predicted on the basis of Eq. 8 and the predicted reverberation times presented in Fig. 24. The predicted spatial variations in the low-frequency regime are based on the measurements made in the model truncated chamber scaled to the 2,135 ft^3 chamber on the basis of modal overlap index. Predictions presented in Fig. 25 indicate that the spatial standard deviation will be approximately 1/2 to 1/4 of a dB less in the concrete wall chamber than in the steel wall chamber.

On the basis of Eq. 14 and the reverberation times presented in Fig. 24, one would expect that approximately 6 dB more sound power level would be required to obtain a given sound pressure level in the steel wall room than in the thick concrete room in the frequency regime below 250 Hz. However Eq. 15 indicates that a given acoustic driver will deliver approximately 6 dB more acoustic power at frequencies below 250 Hz in the steel wall room than in the concrete room. Therefore in the low-frequency regime, the effects of the reverberation times on acoustic power requirements would appear to cancel out. However in the mid-frequency regime (approximately 600 to 2000 Hz),

Eq. 15 indicates that the power delivered by a given driver should be the same in the steel or concrete room and, therefore, in accordance with Eq. 14 the sound pressure level realizable with a given driver should be approximately 5 to 3 dB greater in the concrete room than in the steel wall room.

CONCLUSIONS

The results of this study support the following conclusions:

1. The addition of honeycomb panels to the small chamber did increase the apparent acoustic model density and decrease the spatial variations in the chamber. The panel configuration developed in this study could be utilized to improve the performance of future small reverberation chambers. However the panels could be made more efficient by: (1) using previously developed techniques to enrich the modal dens' f the panels and (2) utilizing baffled pa: with simply supported edges to increase the pan· coupling to the acoustic field.

2. The addition of more absorption to the chamber did decrease the spatial variations at low frequencies, but raised the spatial variations at high frequencies.

3. The electronic feedback techniques did not work for band limited noise excitation because of feedback instability at a single frequency.

4. The use of multiple uncorrelated sources did not decrease the spatial variations measured with one source.

5. The spatial variations in sound pressure level measured in the two small reverberation chambers were relatively small when the modal overlap index of the chambers exceeded one-third.

6. The back effect of a small reverberation chamber on the power output from an acoustic source can be computed based on the modal overlap index of the chamber.

REFERENCES

1. L. W. Sepmeyer, "Computed Frequency and Angular Distribution of the Normal Modes of Vibration in Rectangular Rooms," *J. Acoust. Soc. Am.* 37, 3 (1965).

2. L. L. Beranek, *Noise Reduction* (McGraw-Hill Book Company, Inc., New York, 1960), p. 235.

3. Reference 2, p. 215.

4. P. M. Morse, *Vibration and Sound* (McGraw-Hill Book Company, Inc., New York, 1948), Section 32.

5. R. H. Bolt and R. W. Roop, "Frequency Response Fluctuations in Rooms," *J. Acoust. Soc. Am.*, 22, 2 (1956).

6. M. K. Schroeder, "Effect of Frequency and Space Averaging on the Transmission Responses of Multimode Media," *J. Acoust. Soc. Am.*, 46, 2 (1969).

7. R. H. Lyon, "Statistical Analysis of Power Injection and Response in Structures and Rooms," *J. Acoust. Soc. Am.* 45, 3 (1969).

8. R. H. Lyon and G. Maidanik, "Power Flow between Linearly Coupled Oscillators," *J. Acoust. Soc. Am.*, 34, 5 (1961).

9. J. E. Manning, R. H. Lyon and T. D. Scharton, "Transmission of Sound and Vibration to a Shroud Enclosed Spacecraft," BBN Report 1413, submitted to NASA Goddard Space Flight Center, Greenbelt, Maryland, under Contract No. NAS5-9001 (15 October 1966),Eq. 23.

10. E. E. Ungar and T. D. Scharton, "Analysis of Vibration Distributions in Complex Structures," *Shock and Vibration Bulletin* 36, 5 (January 1967), Table 1.

11. T. D. Scharton and T. M. Yang, "Substitute Acoustic Tests," *Shock and Vibration Bulletin* 38, 1 (1969).

12. T. D. Scharton, "Development of an Impedance Simulation Vibration Test Fixture for Spacecraft Vibration Tests," *Shock and Vibration Bulletin*, 40, 1 (1970).

13. T. D. Scharton, "Development of Improved Vibration Tests of Spacecraft Assemblies," BBN Report 1702, submitted to Jet Propulsion Laboratory, Pasadena, California (1968).

14. L. L. Beranek, *Acoustics* (McGraw-Hill Book Company, Inc., New York, 1954).

15. Reference 2, p.

16. Reference 2, p. 24.

17. American Standards Association, "American Standard Method for the Physical Measurement of Sound," S1. 2-1962, Eq. 16b.

18. J. F. Mills, "A Study of Reverberation Chamber Characteristics," Institute of Environmental Sciences 1967 Proceedings, Fig. 10.

19. T. D. Scharton and P. H. Smith, "The Average Resistance and Conductance of Vibratory and Acoustic Systems," to be published in the *J. Acoust. Soc. Am.*

20. Private communication with Mr. David Smith, Aerosonics Laboratory, Wright-Patterson Air Force Base.

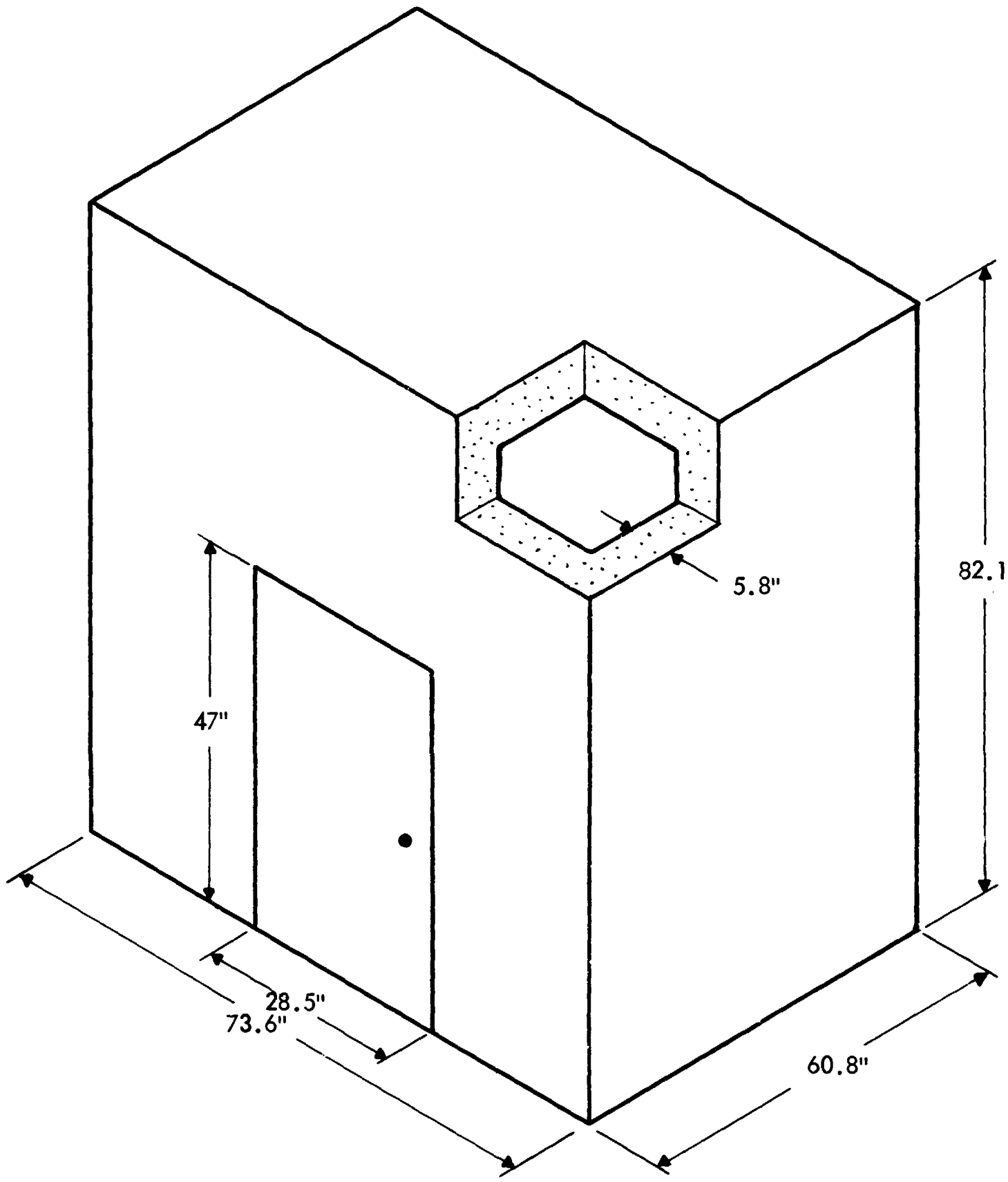

Inside Dimensions

Height - 76.3 inches
Depth - 49.2 inches
Width - 62.0 inches
Volume - 135 feet ^{3}
Area - 160.5 feet ^{2}

FIGURE 1. RECTANGULAR CHAMBER

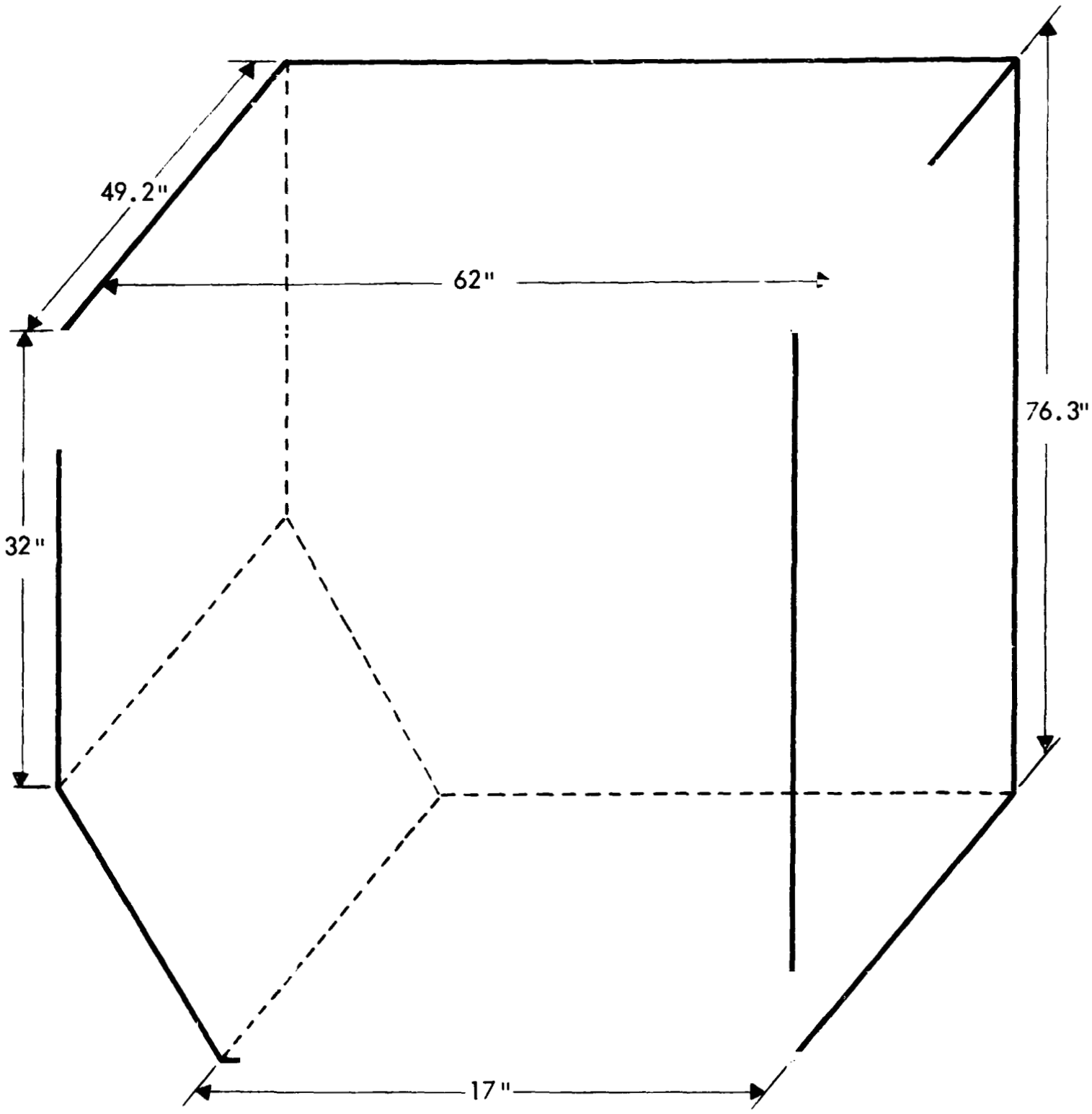

FIGURE 2. INSIDE DIMENSIONS OF TRUNCATED CHAMBER

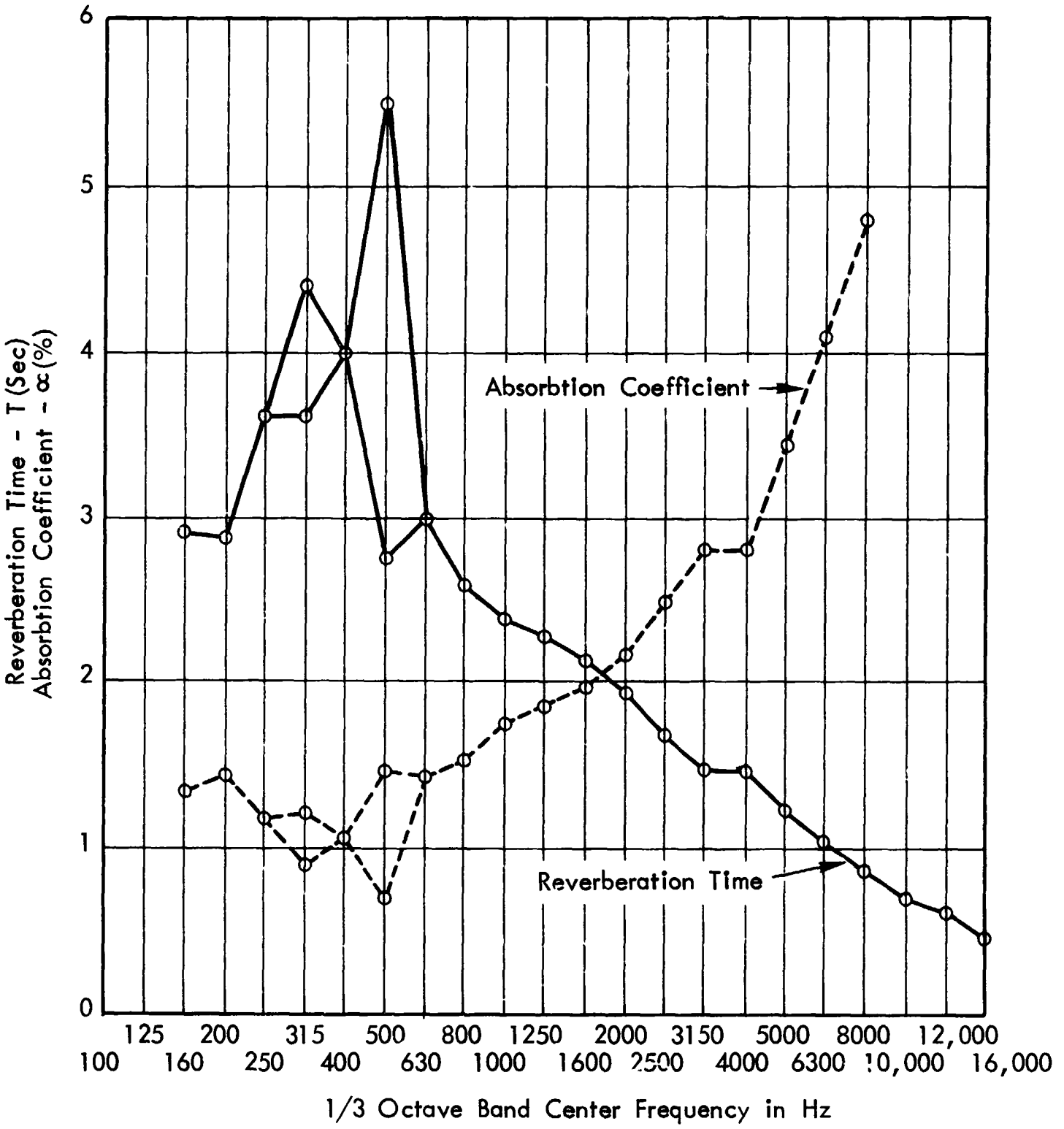

FIGURE 3. REVERBERATION TIME AND ABSORBTION COEFFICIENT OF RECTANGULAR CHAMBER

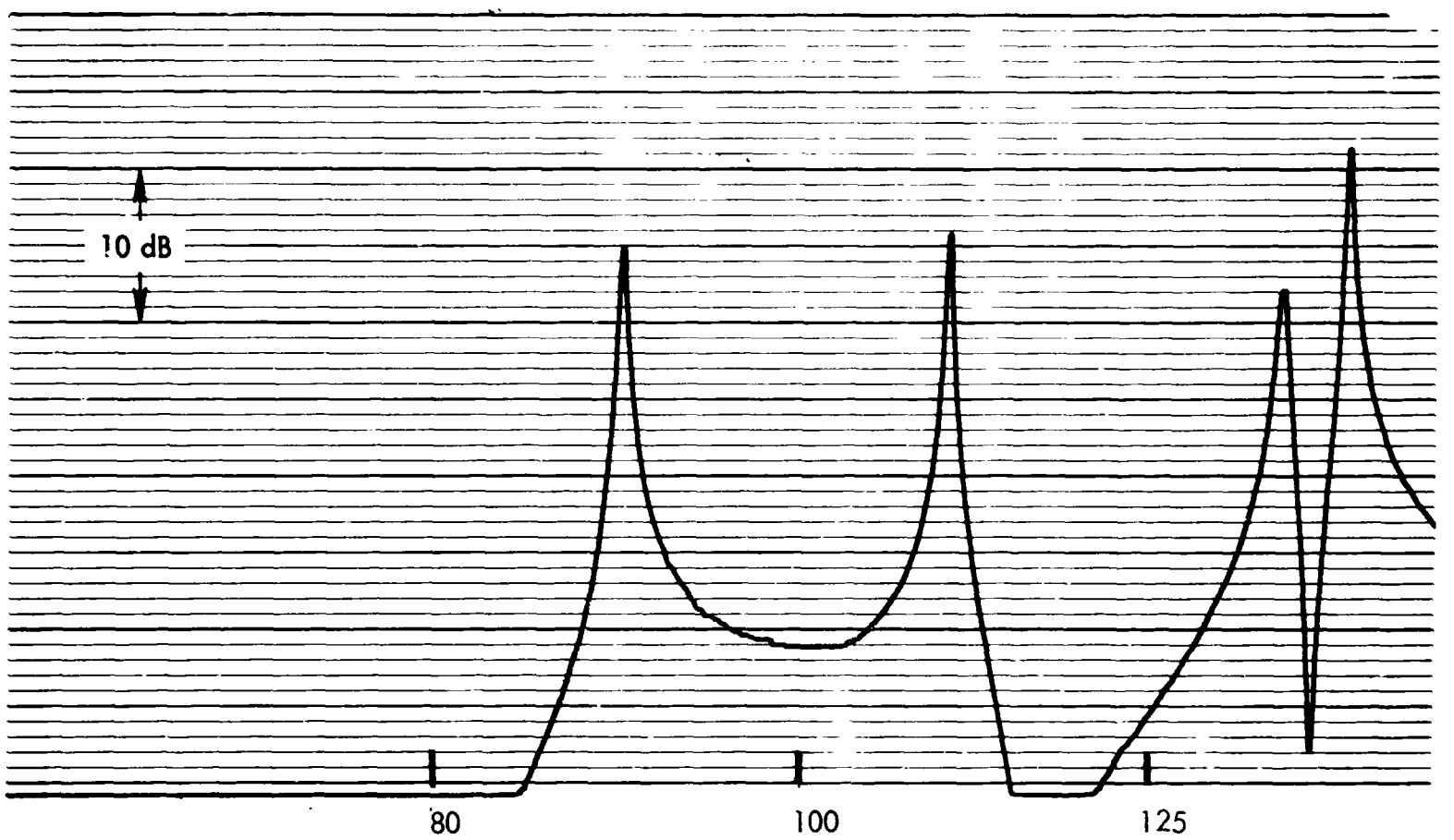

FIGURE 4a. SINE SWEEP RESPONSE (80-125 Hz)
RECTANGULAR CHAMBER

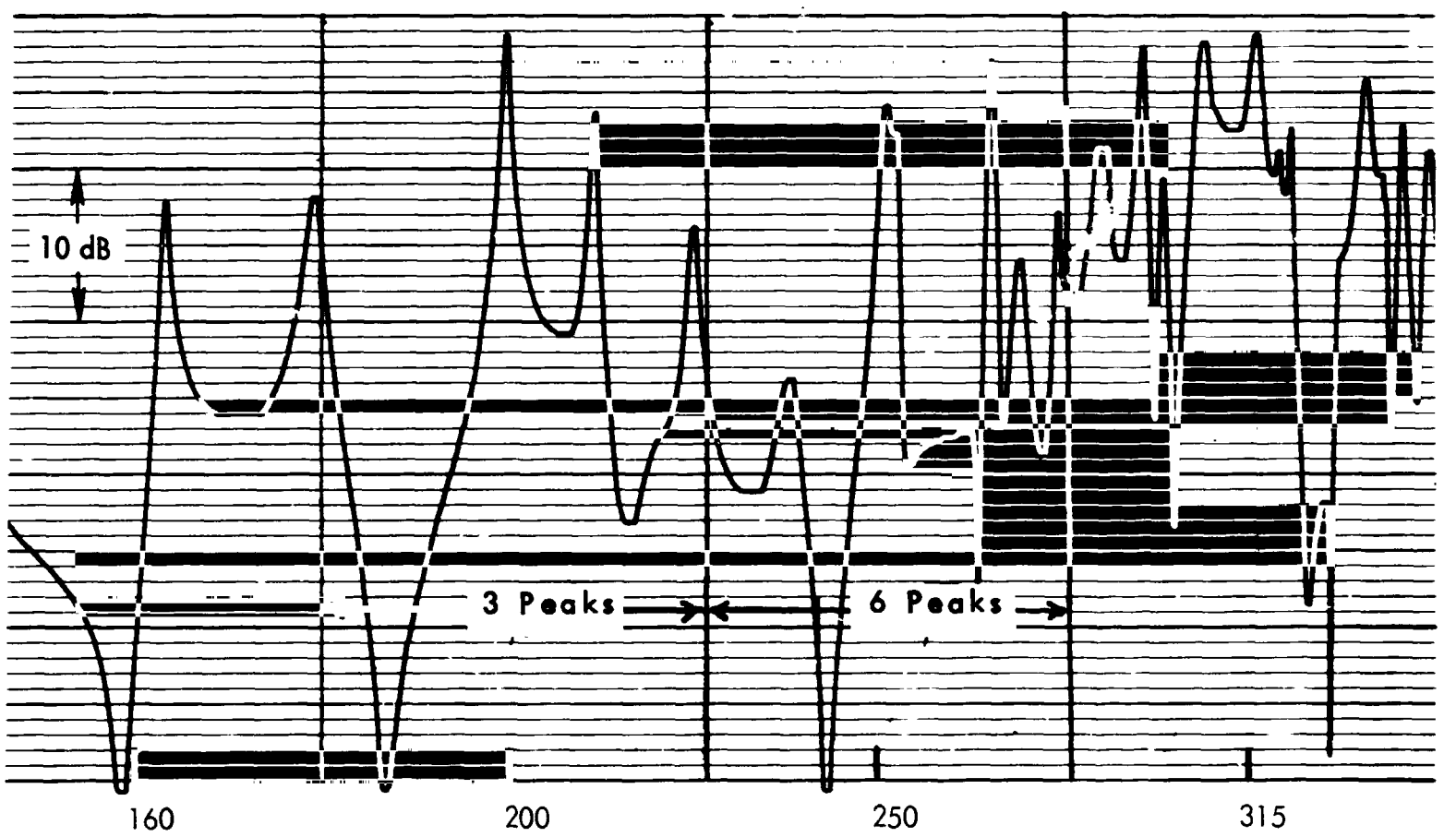

FIGURE 4b. SINE SWEEP RESPONSE (160-315 Hz)
RECTANGULAR CHAMBER

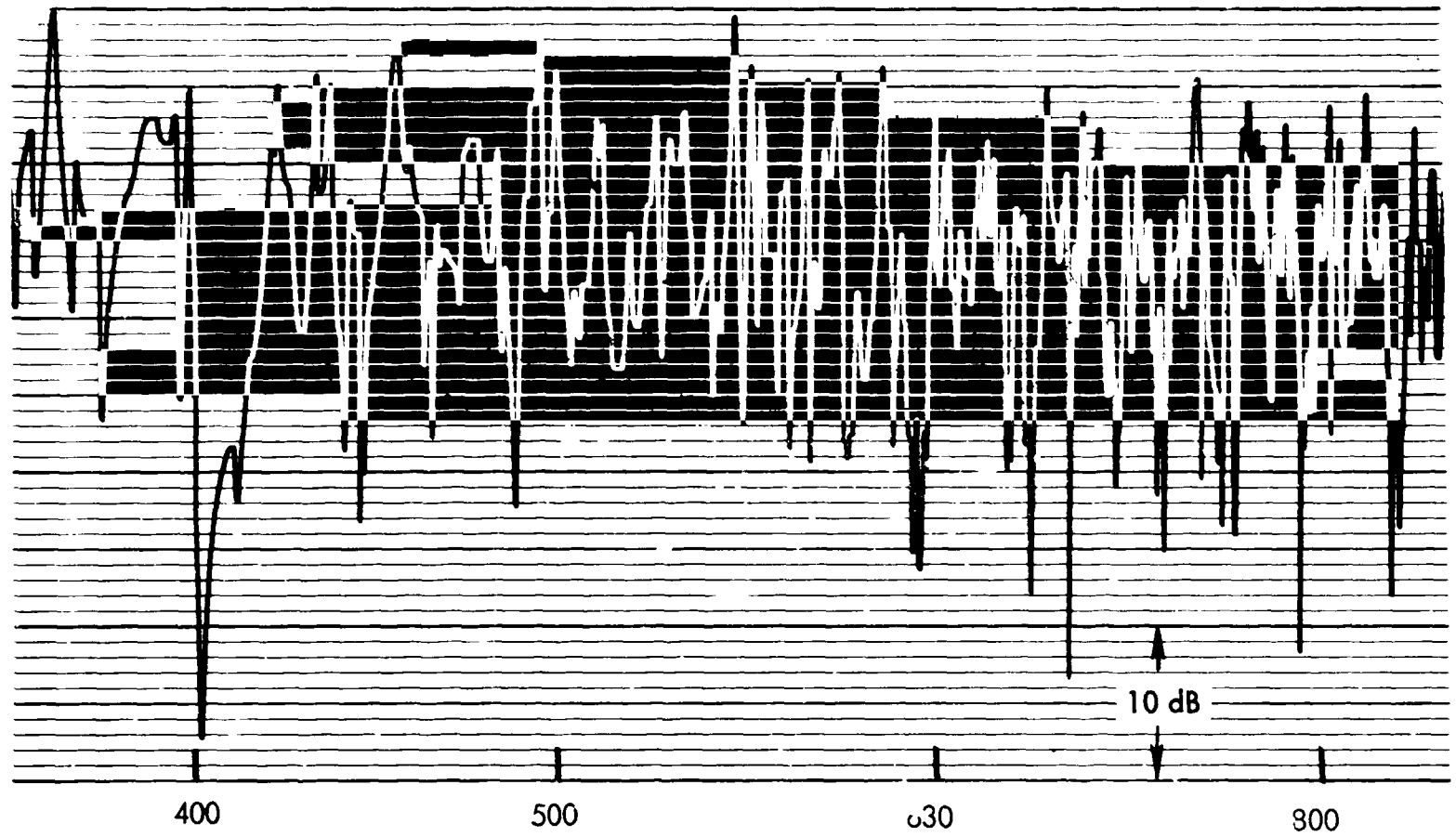

FIGURE 4c. SINE SWEEP RESPONSE (400-800 Hz)
RECTANGULAR CHAMBER

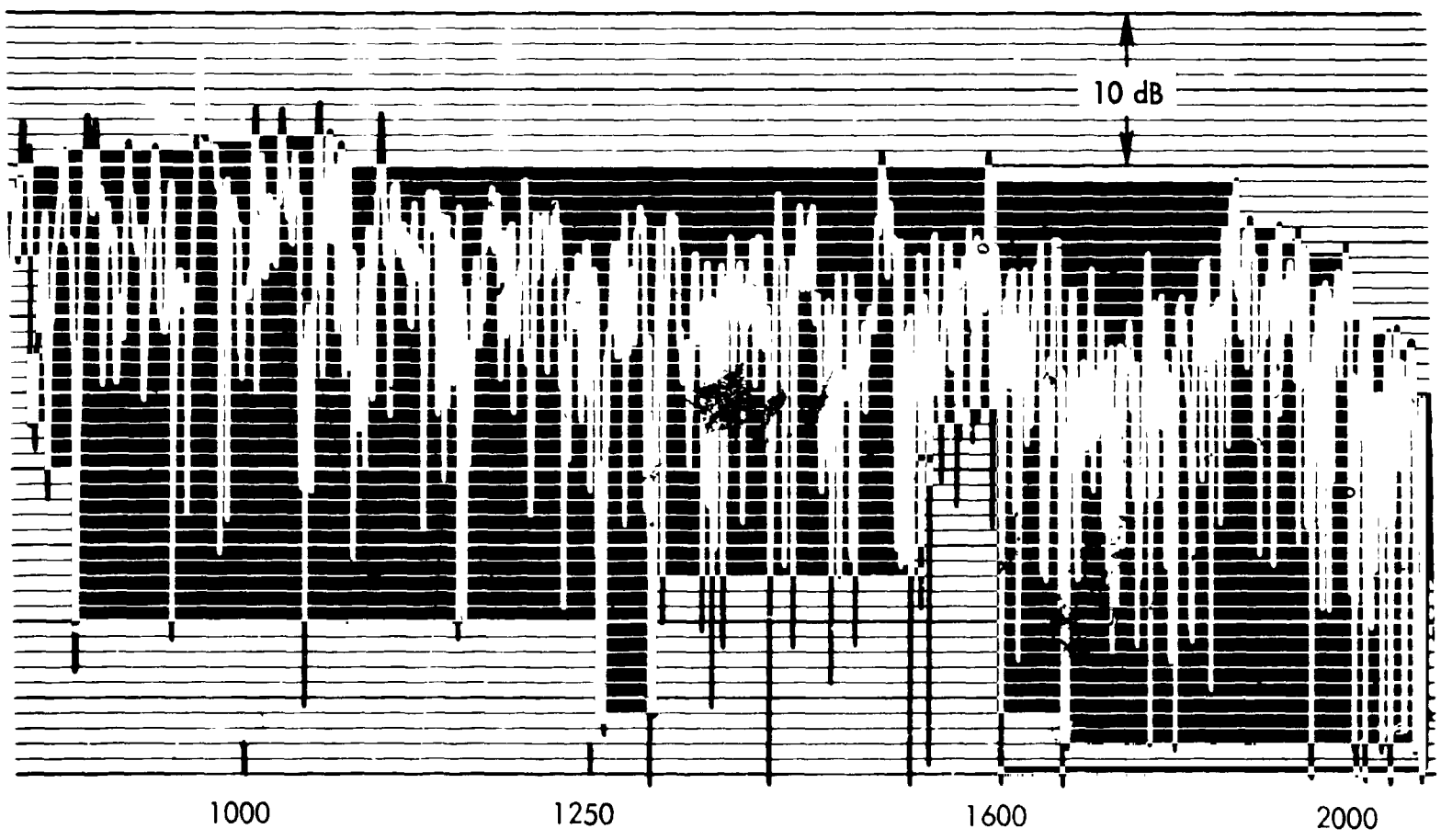

FIGURE 4d. SINE SWEEP RESPONSE (1000-2000 Hz)
RECTANGULAR CHAMBER

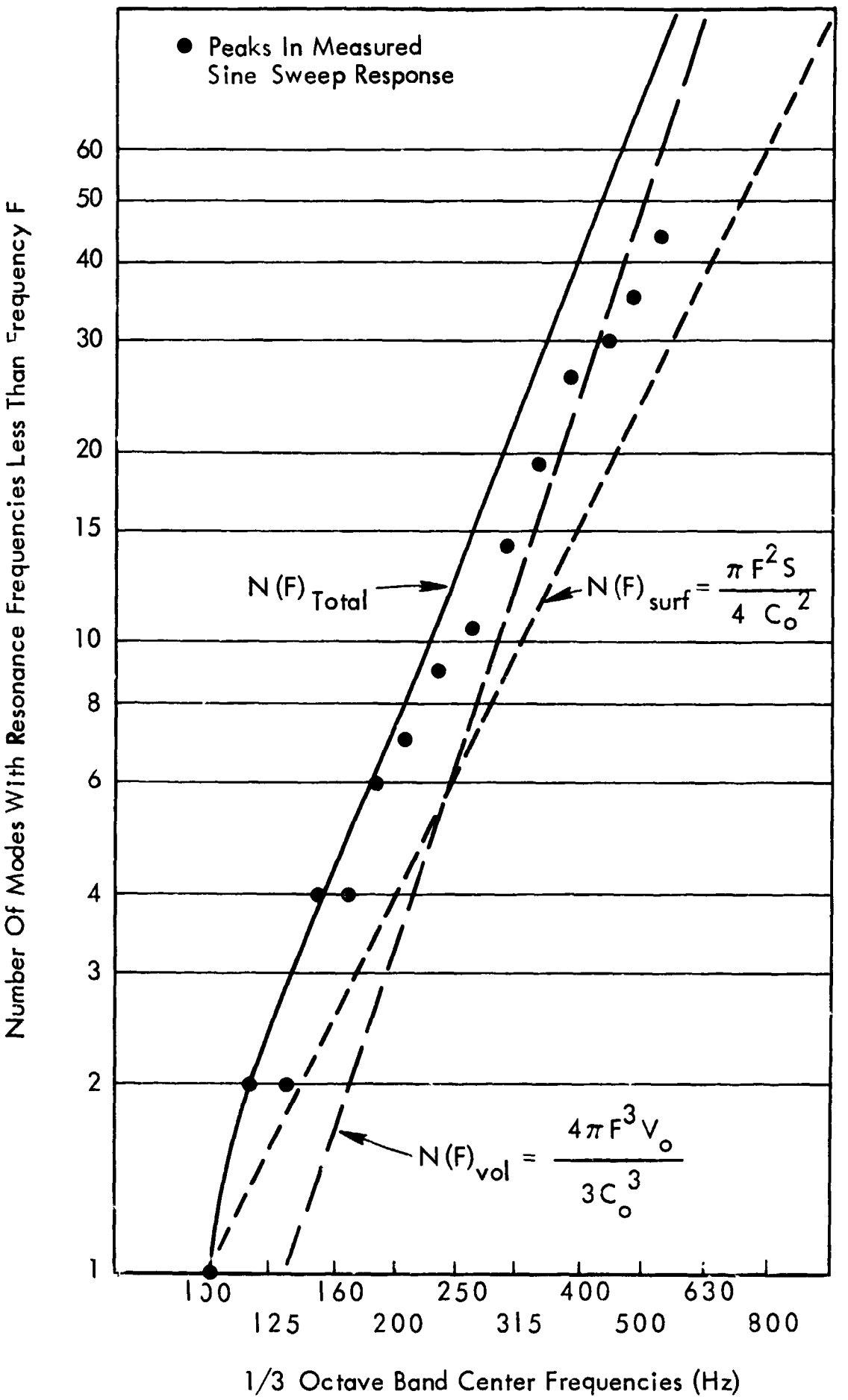

FIGURE 5. COMPARISON OF MEASURED AND PREDICTED MODE COUNTS FOR RECTANGULAR CHAMBER

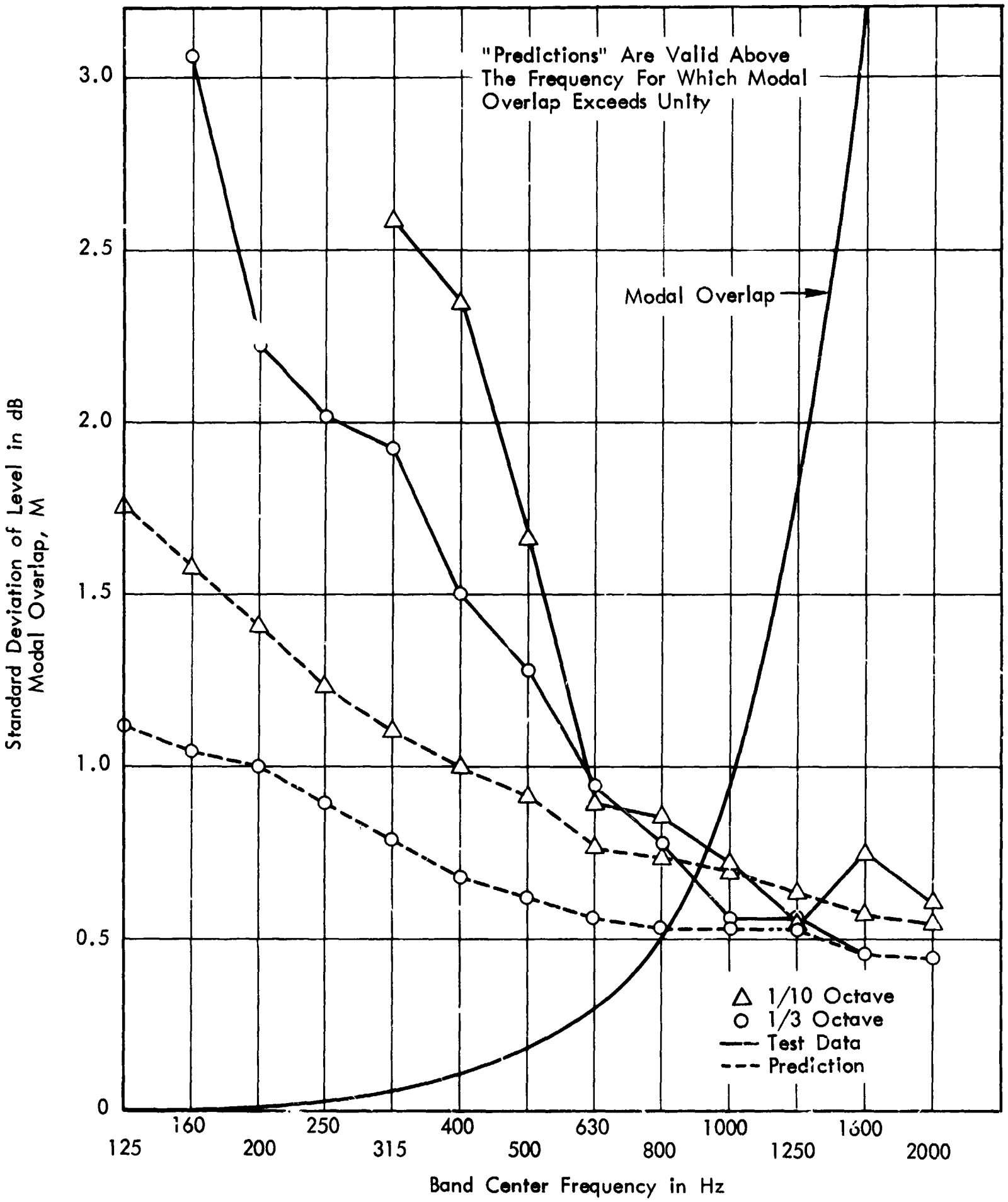

FIGURE 6. SPATIAL VARIATIONS IN RECTANGULAR CHAMBER

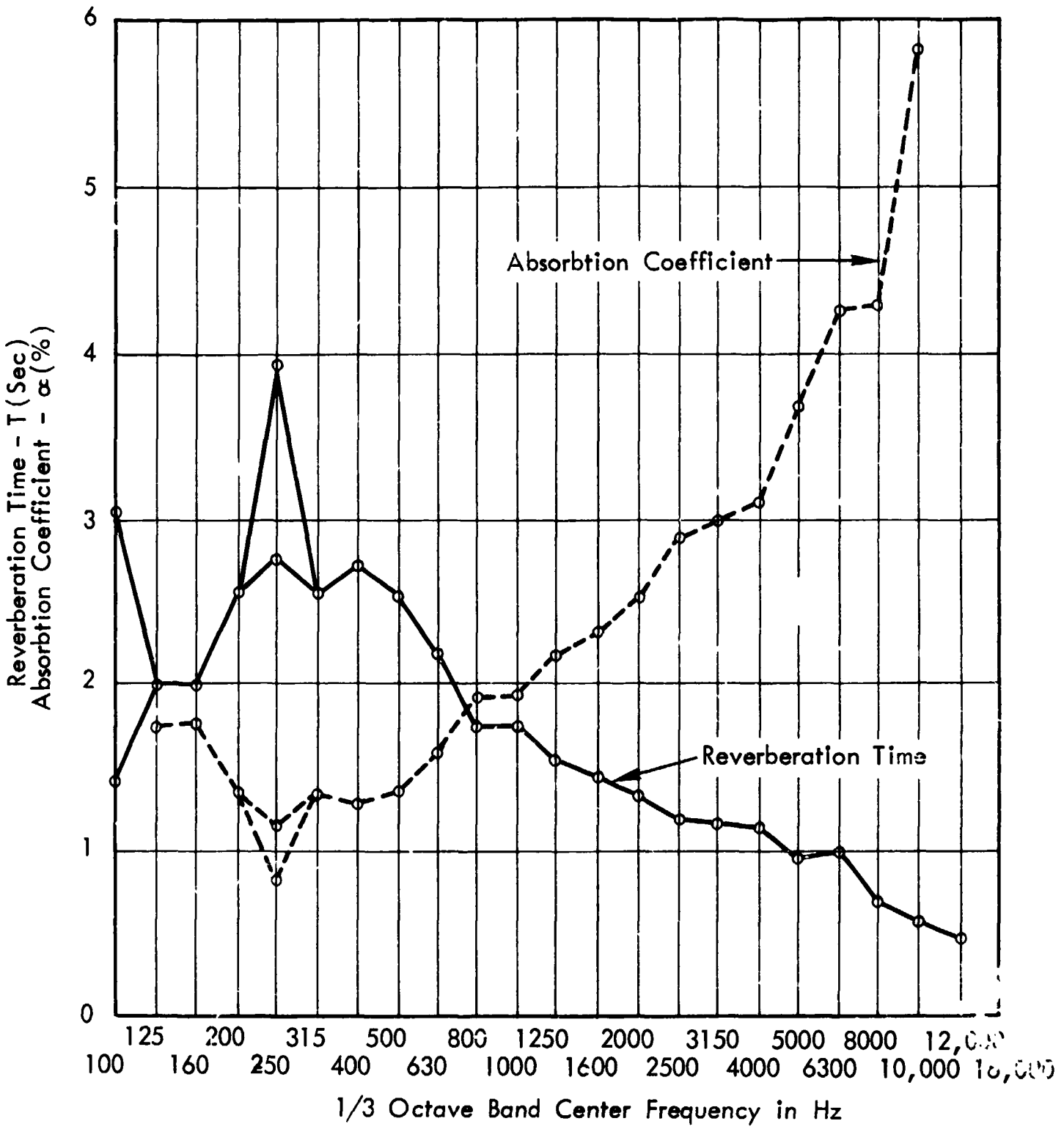

FIGURE 7. REVERBERATION TIME AND ABSORBTION COEFFICIENT OF TRUNCATED CHAMBER

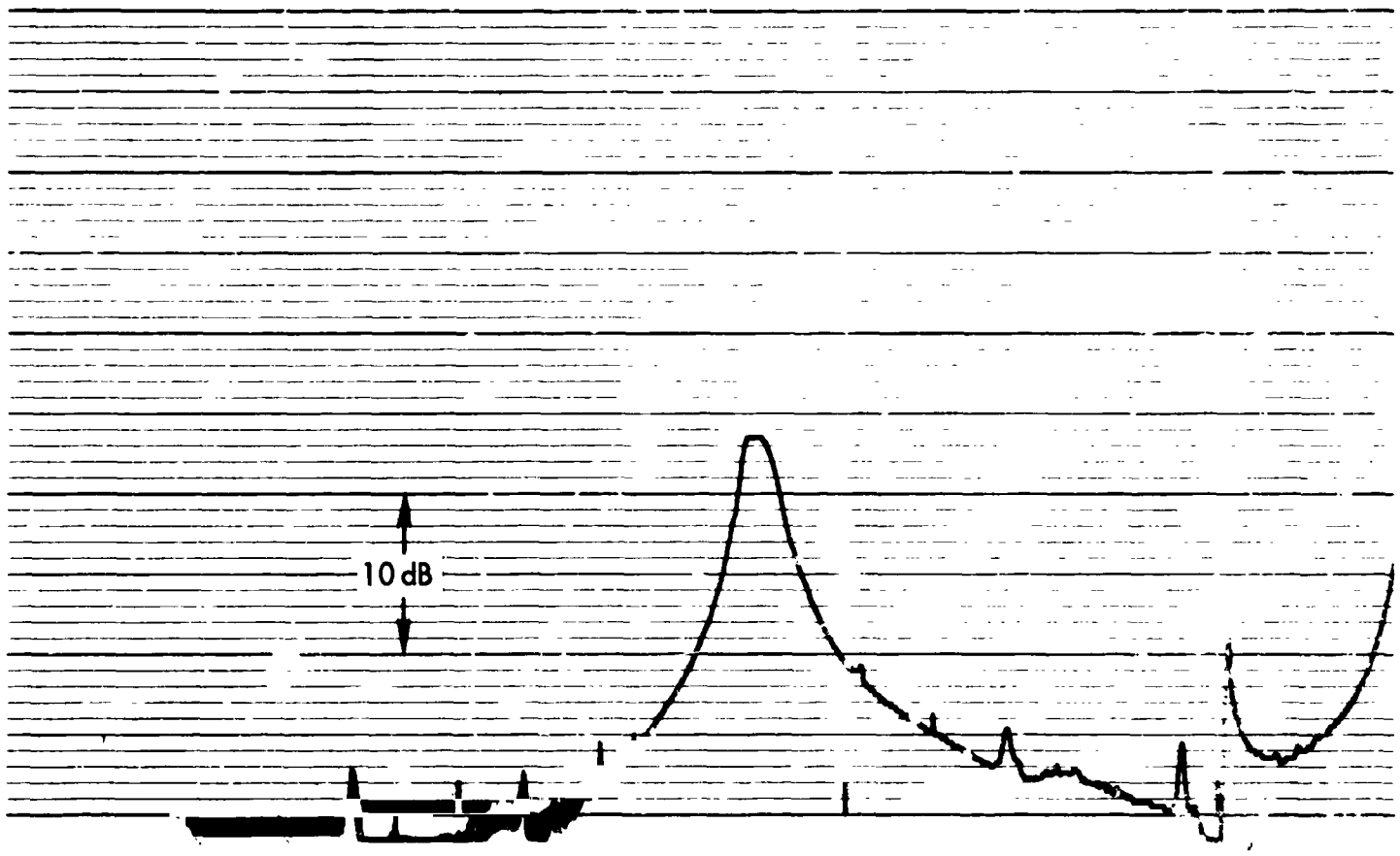

FIGURE 8a. SINE SWEEP RESPONSE (80-125 Hz)
TRUNCATED REVERBERATION CHAMBER

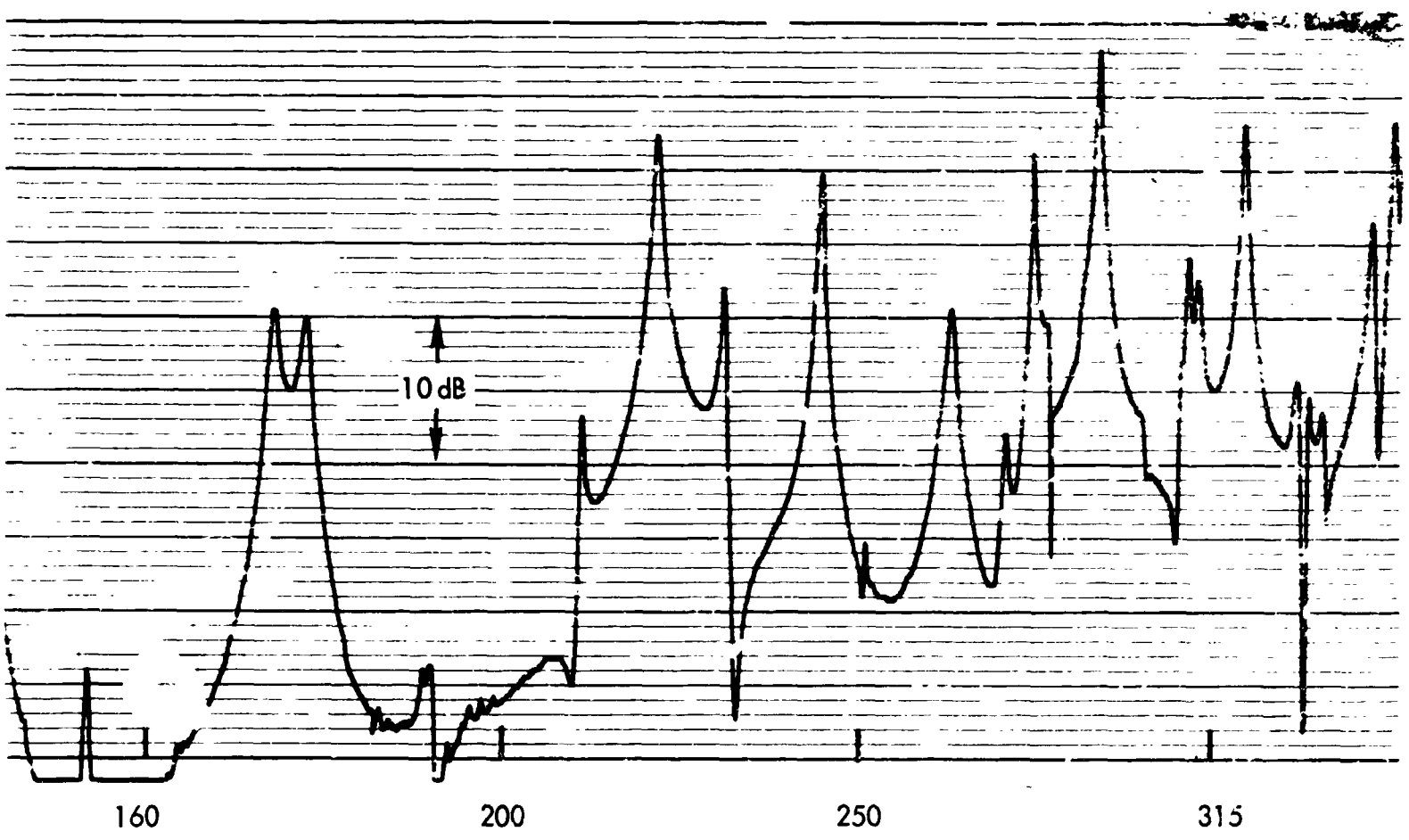

FIGURE 8b. SINE SWEEP RESPONSE (160-315 Hz)
TRUNCATED REVERBERATION CHAMBER

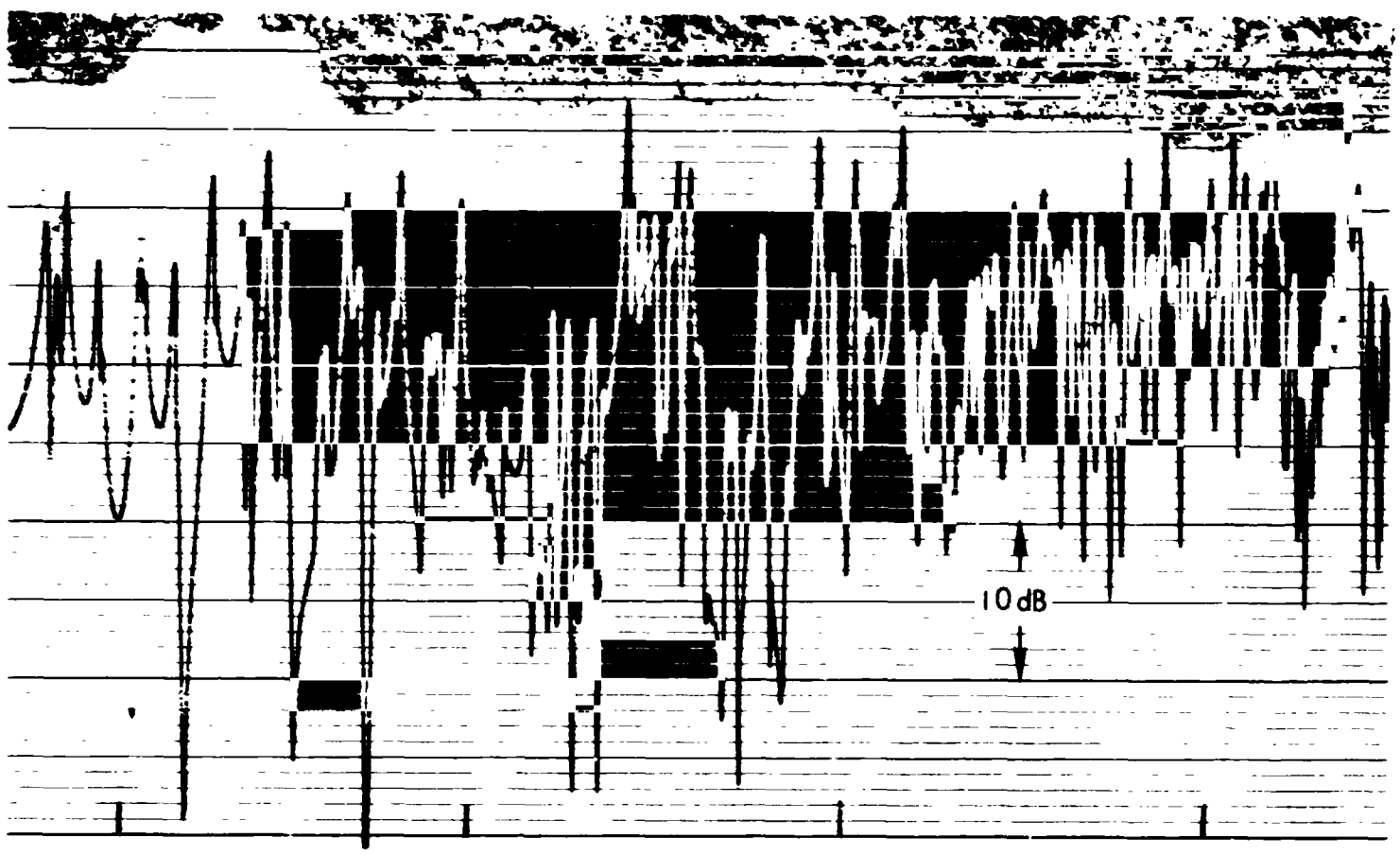

FIGURE 8c. SINE SWEEP RESPONSE (400-800 Hz)
TRUNCATED REVERBERATION CHAMBER

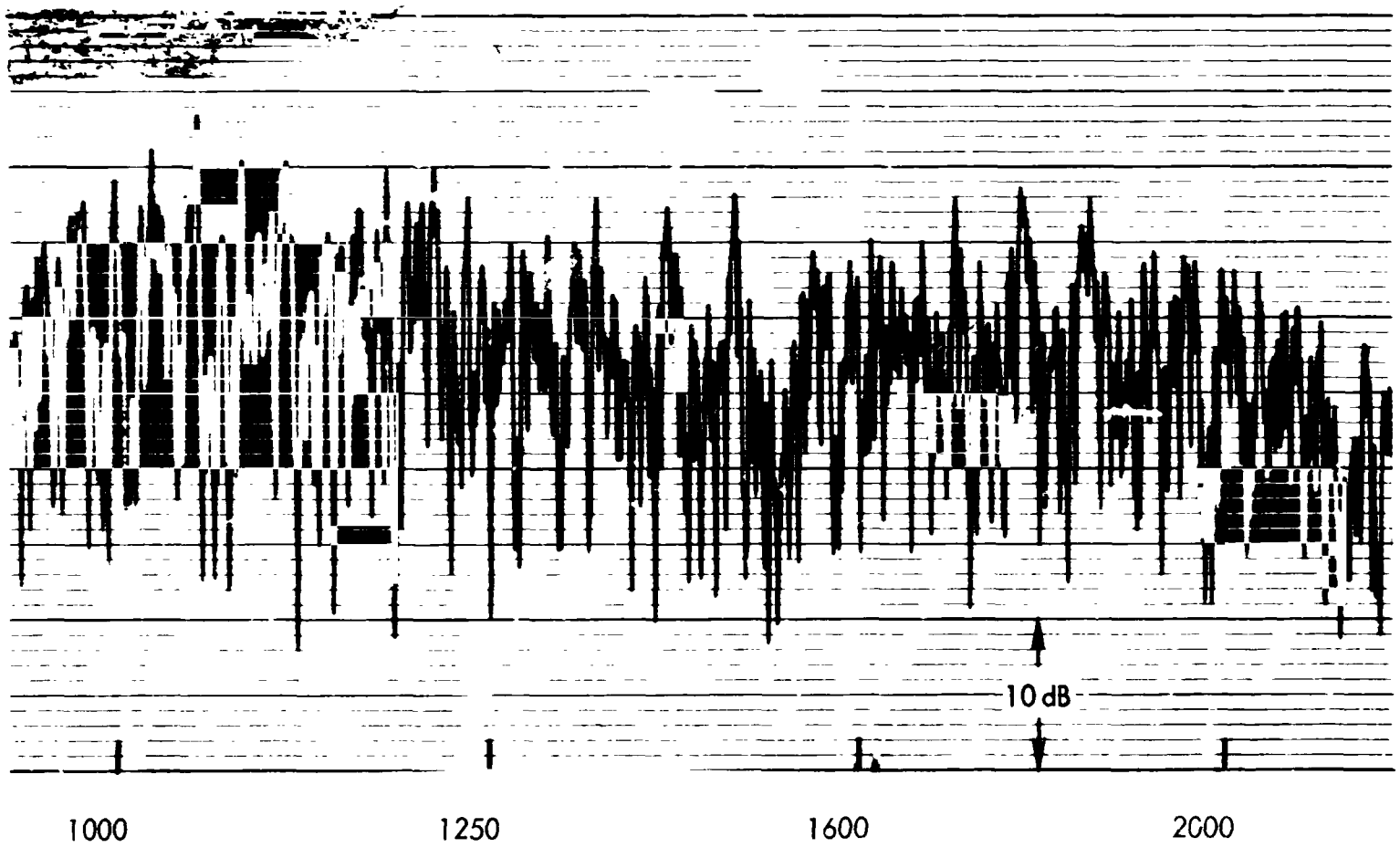

FIGURE 8d. SINE SWEEP RESPONSE (1000-2000 Hz)
TRUNCATED RE /ERBERATION CHAMBER

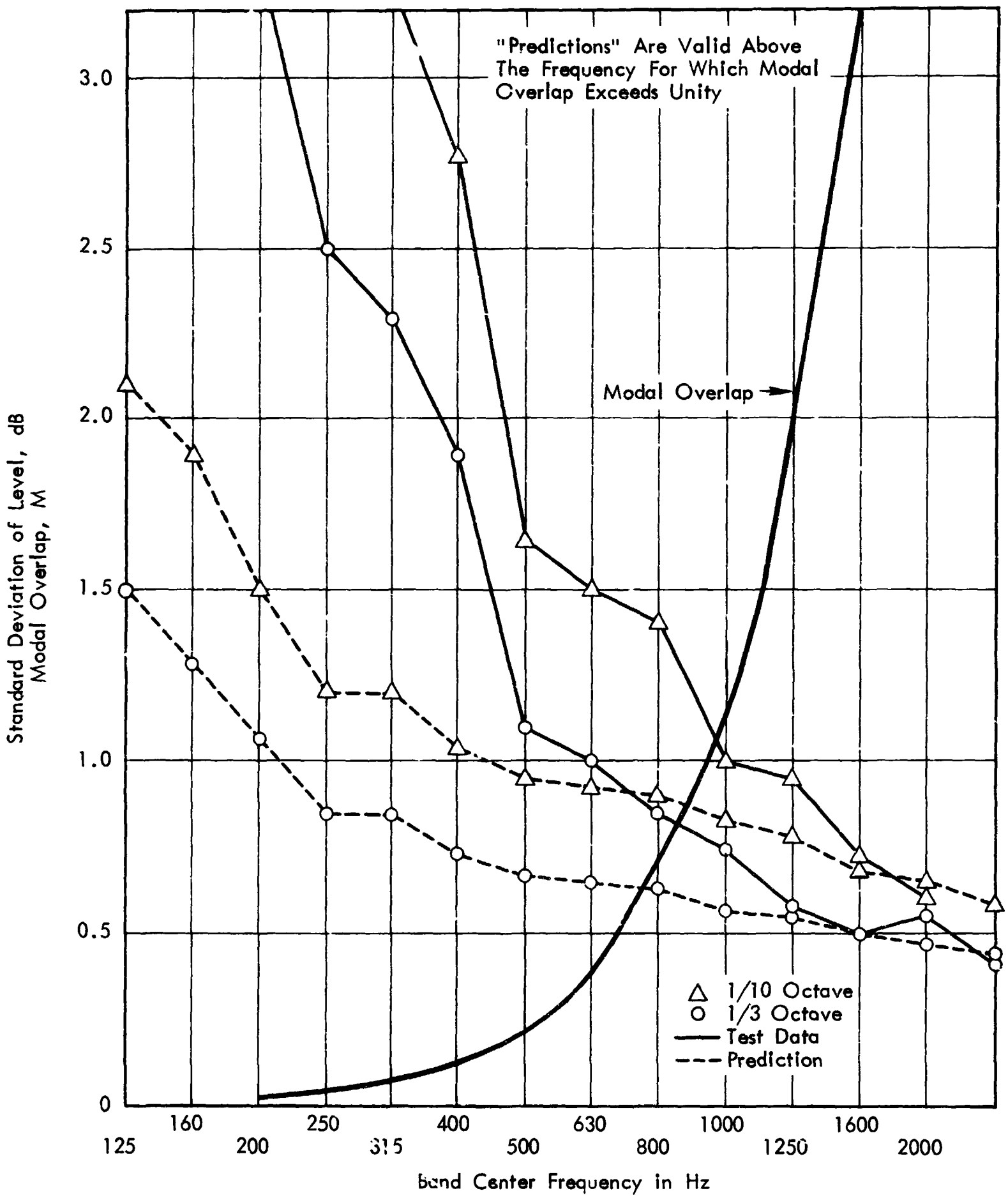

FIGURE 9. SPATIAL VARIATIONS IN TRUNCATED CHAMBER

HONEYCOMB
CROSS SECTION

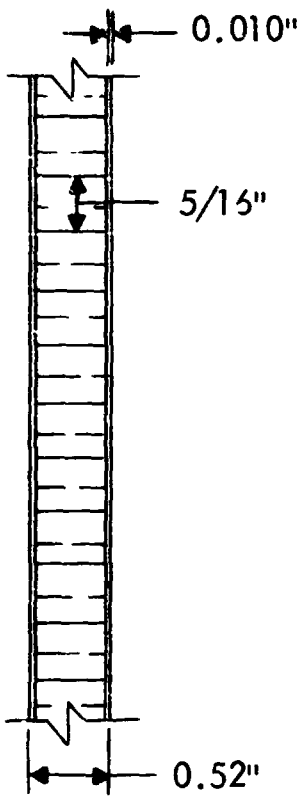

PANEL DENSITY

Surface	0.24	lb/ft^2
Core	0.16	lb/ft^2
Adhesive	0.03	lb/ft^2
Total	0.43	lb/ft^2

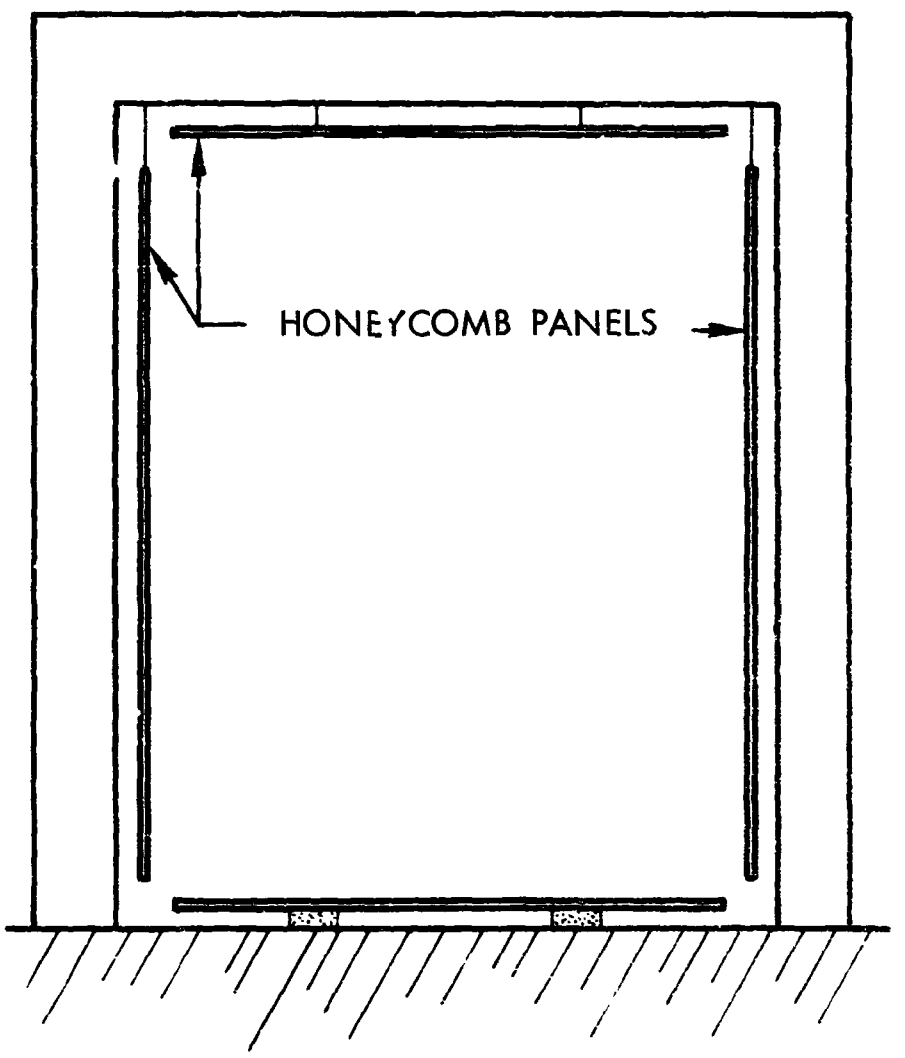

FIGURE 10. HONEYCOMB PANELS IN CHAMBER

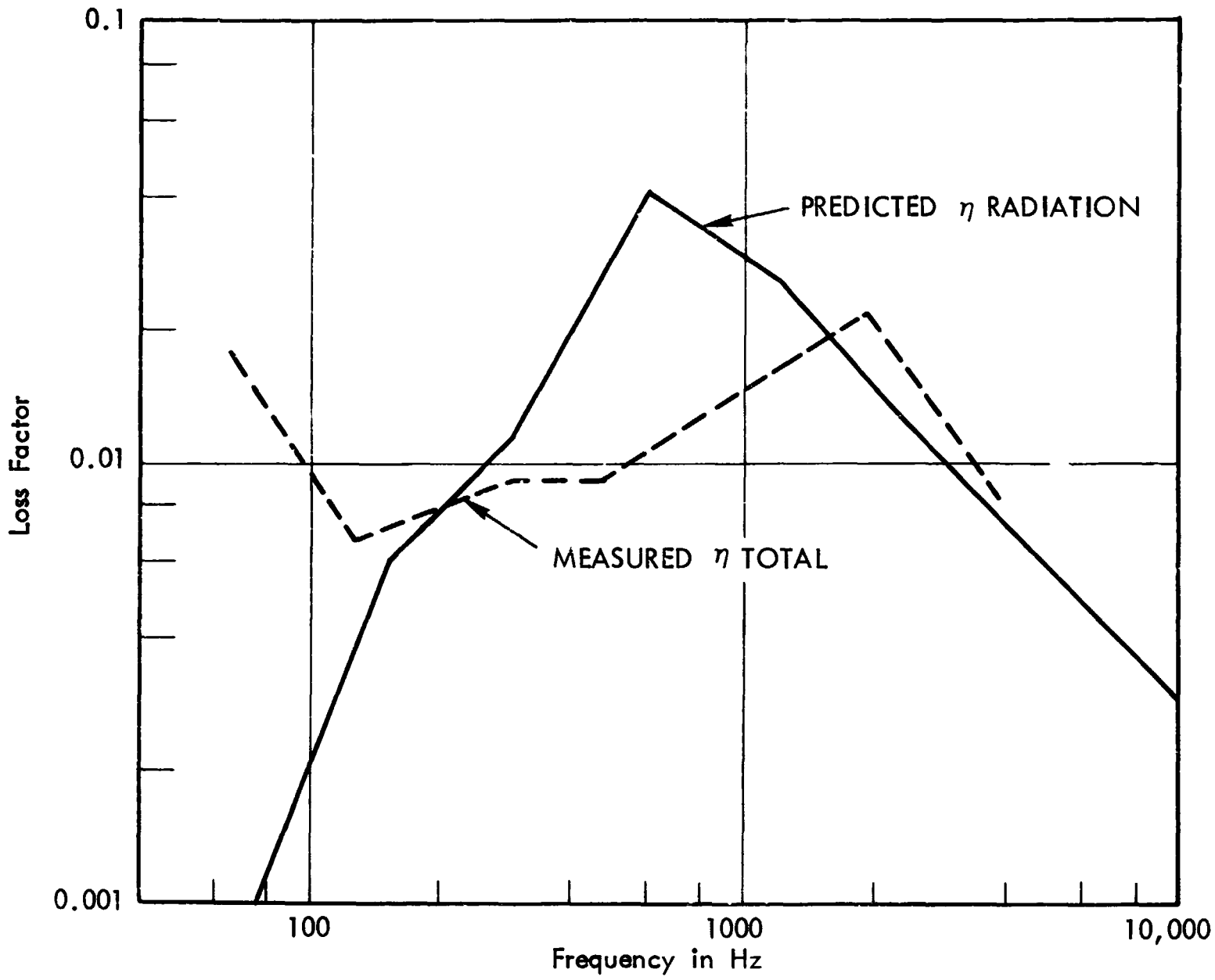

FIGURE 11. PREDICTED RADIATION AND MEASURED TOTAL LOSS FACTORS OF 2' x 5' x 1/2" HONEYCOMB PANEL

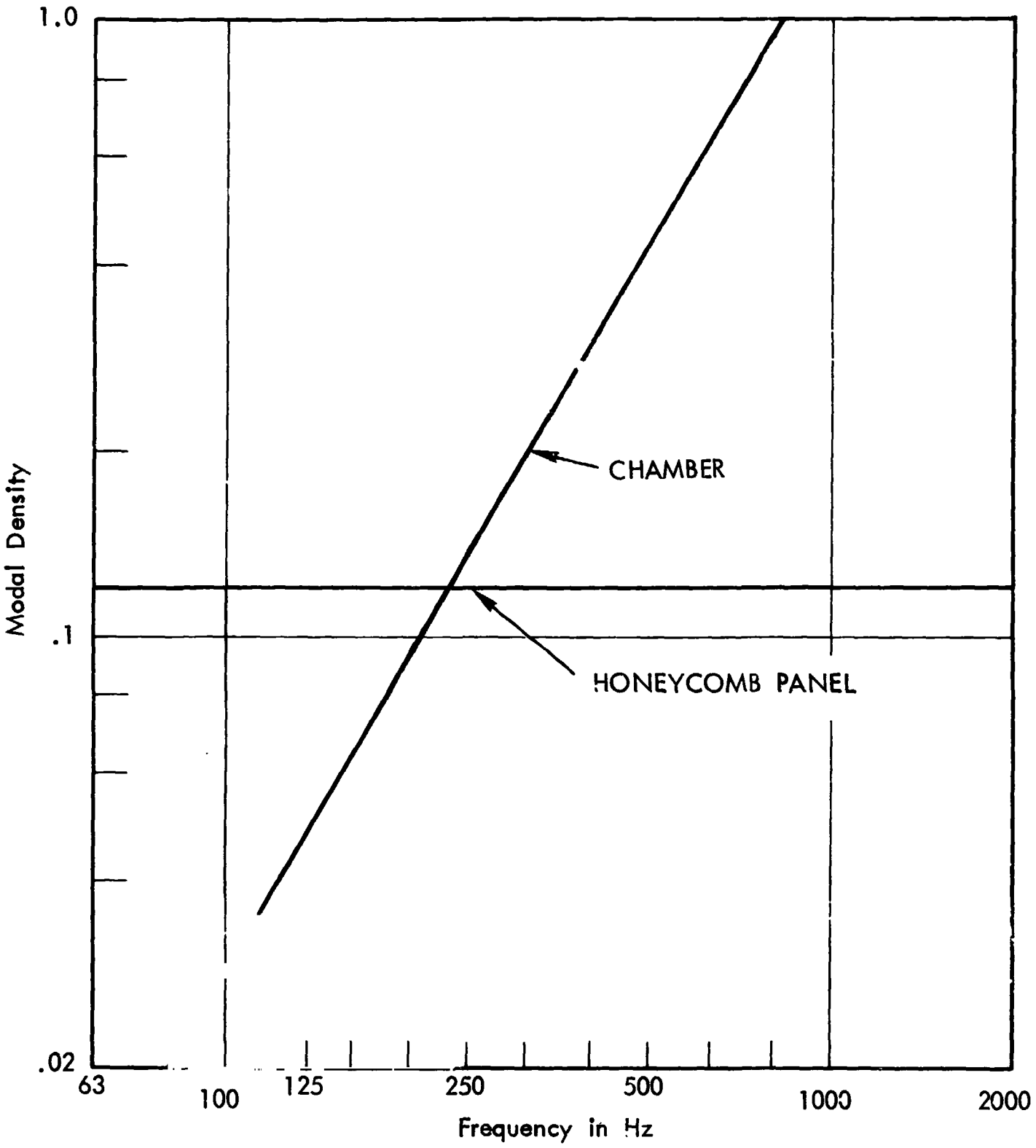

FIGURE 12. MODAL DENSITIES OF HONEYCOMB PANELS AND RECTANGULAR CHAMBER

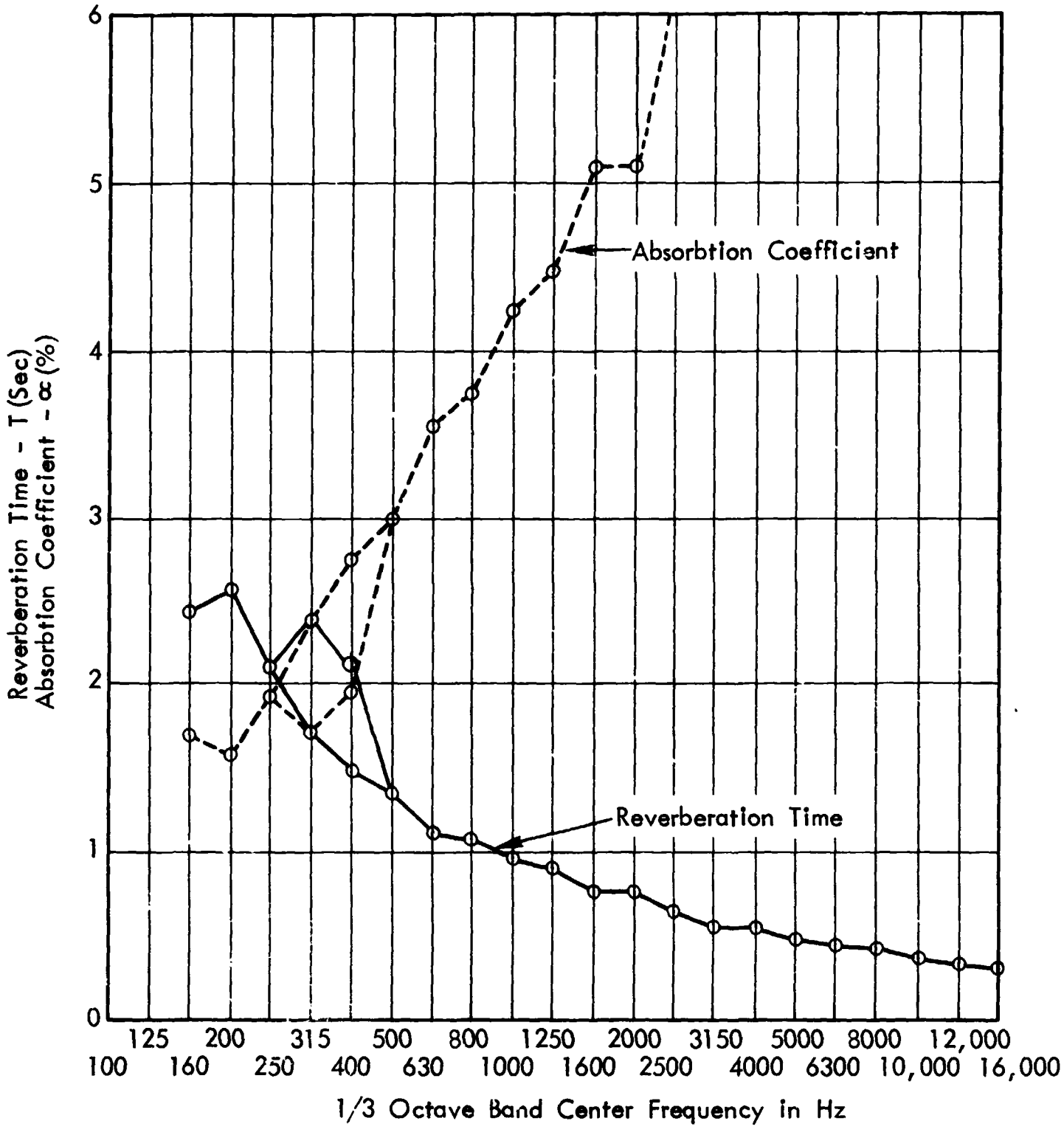

FIGURE 13. REVERBERATION TIME AND ABSORBTION COEFFICIENT OF RECTANGULAR CHAMBER WITH MODAL ENRICHMENT PANELS

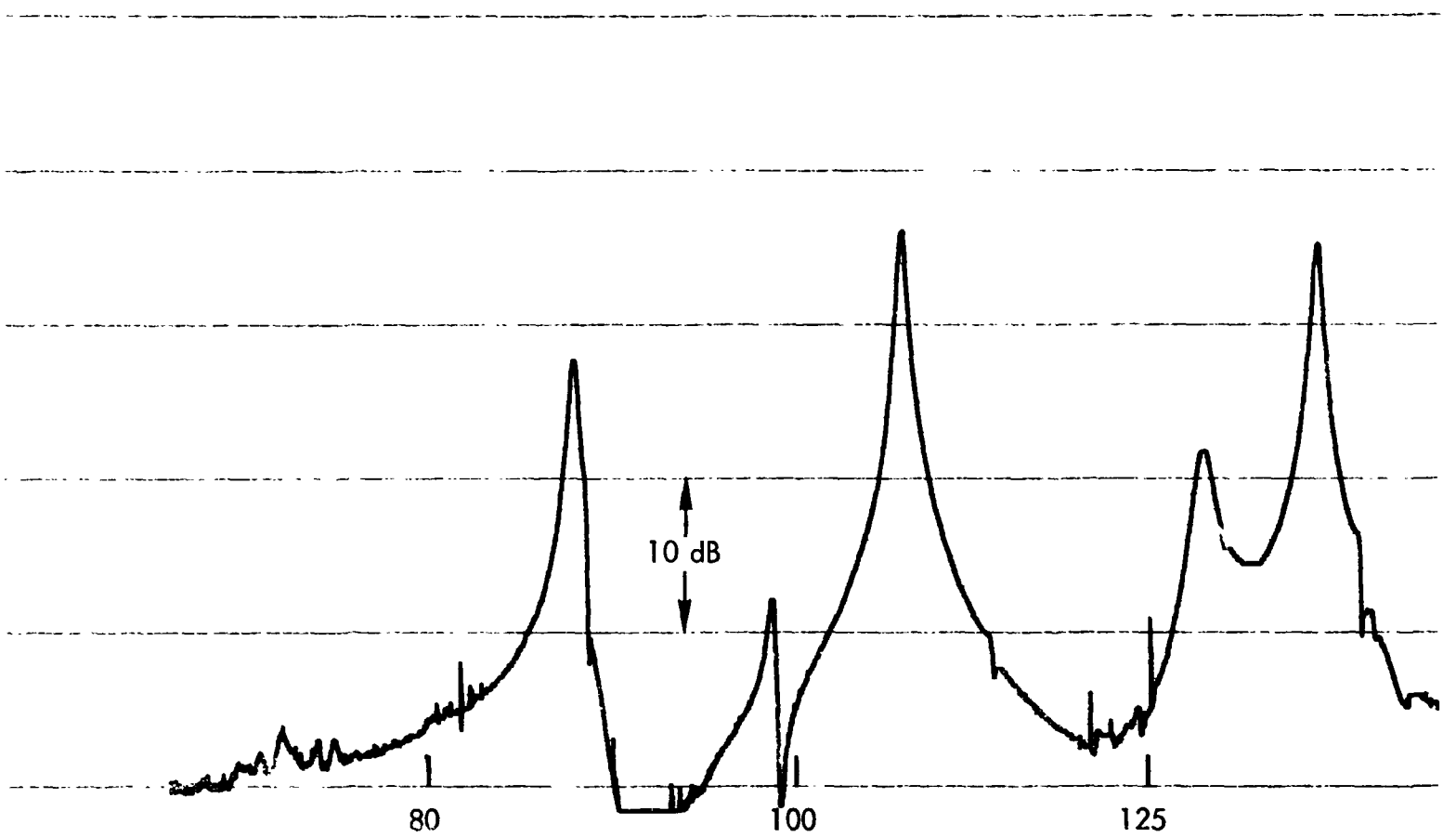

FIGURE 14a. SINE SWEEP RESPONSE (80-125 Hz)
RECTANGULAR CHAMBER WITH MODAL ENRICHMENT PANELS

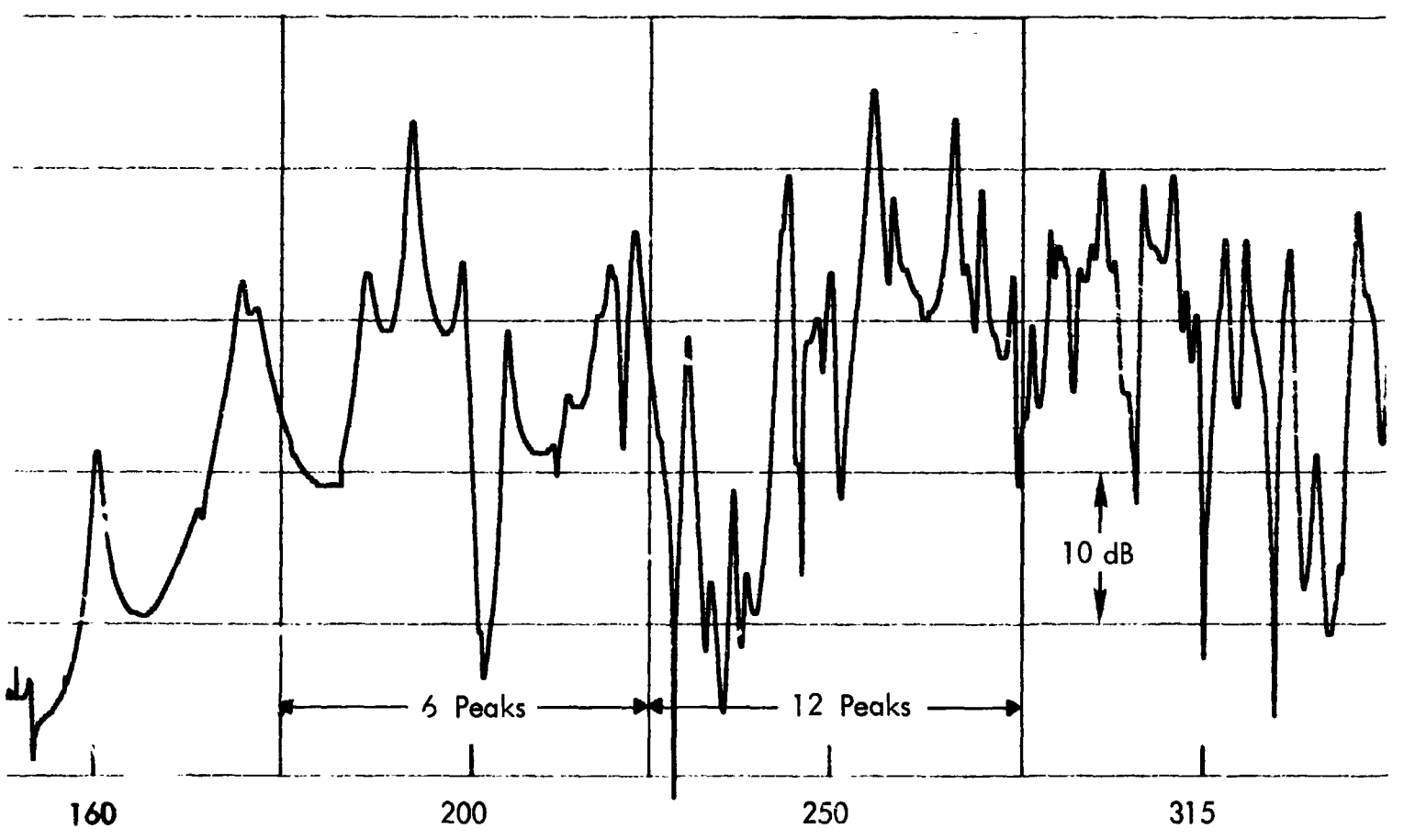

FIGURE 14b. SINE SWEEP RESPONSE (160-315 Hz)
RECTANGULAR CHAMBER WITH MODAL ENRICHMENT PANELS

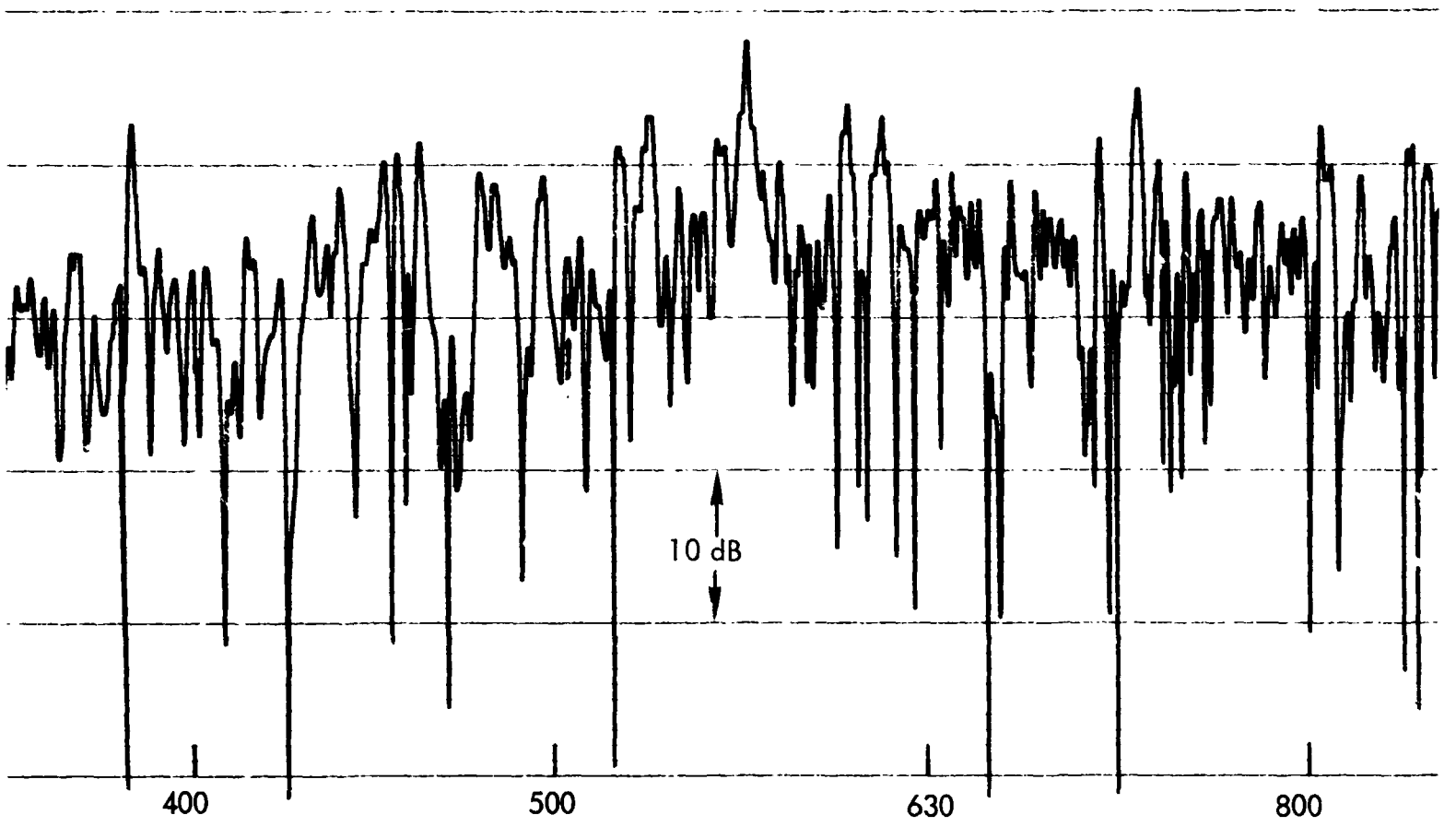

FIGURE 14c. SINE SWEEP RESPONSE (400-800 Hz)
RECTANGULAR CHAMBER WITH MODAL ENRICHMENT PANELS

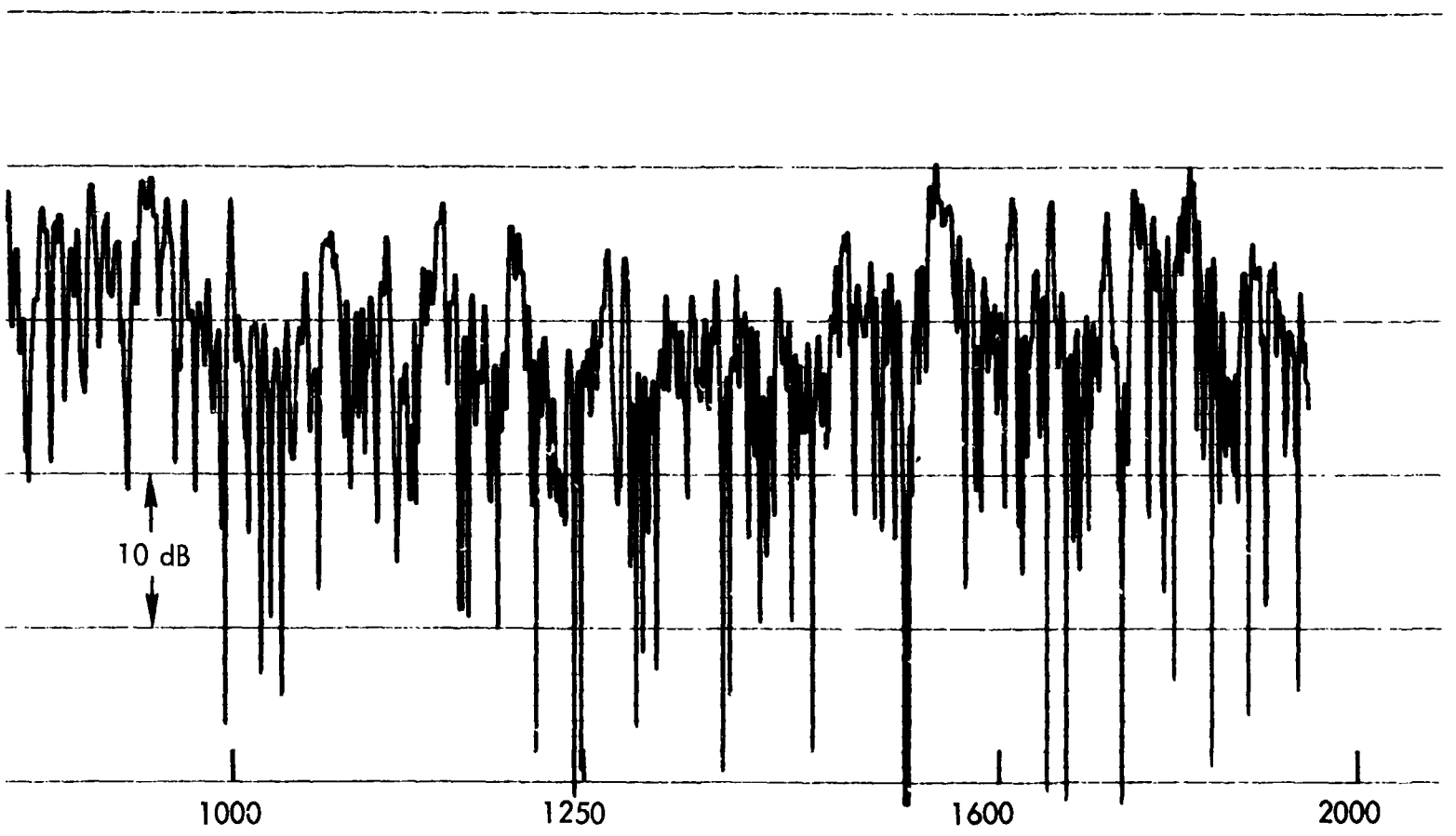

FIGURE 14d. SINE SWEEP RESPONSE (1000-2000 Hz)
RECTANGULAR CHAMBER WITH MODAL ENRICHMENT PANELS

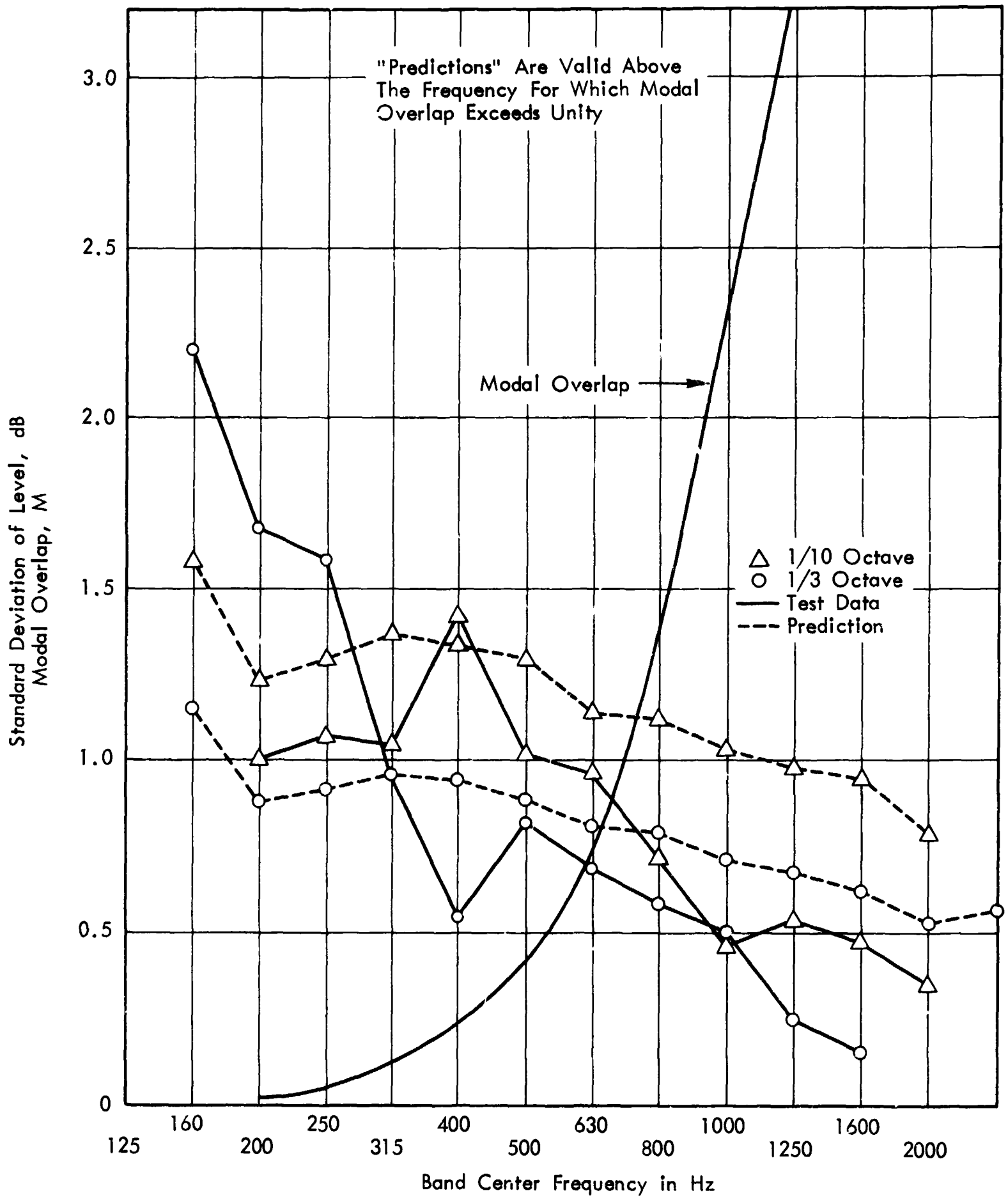

FIGURE 15. SPATIAL VARIATIONS IN RECTANGULAR CHAMBER WITH HONEYCOMB PANELS

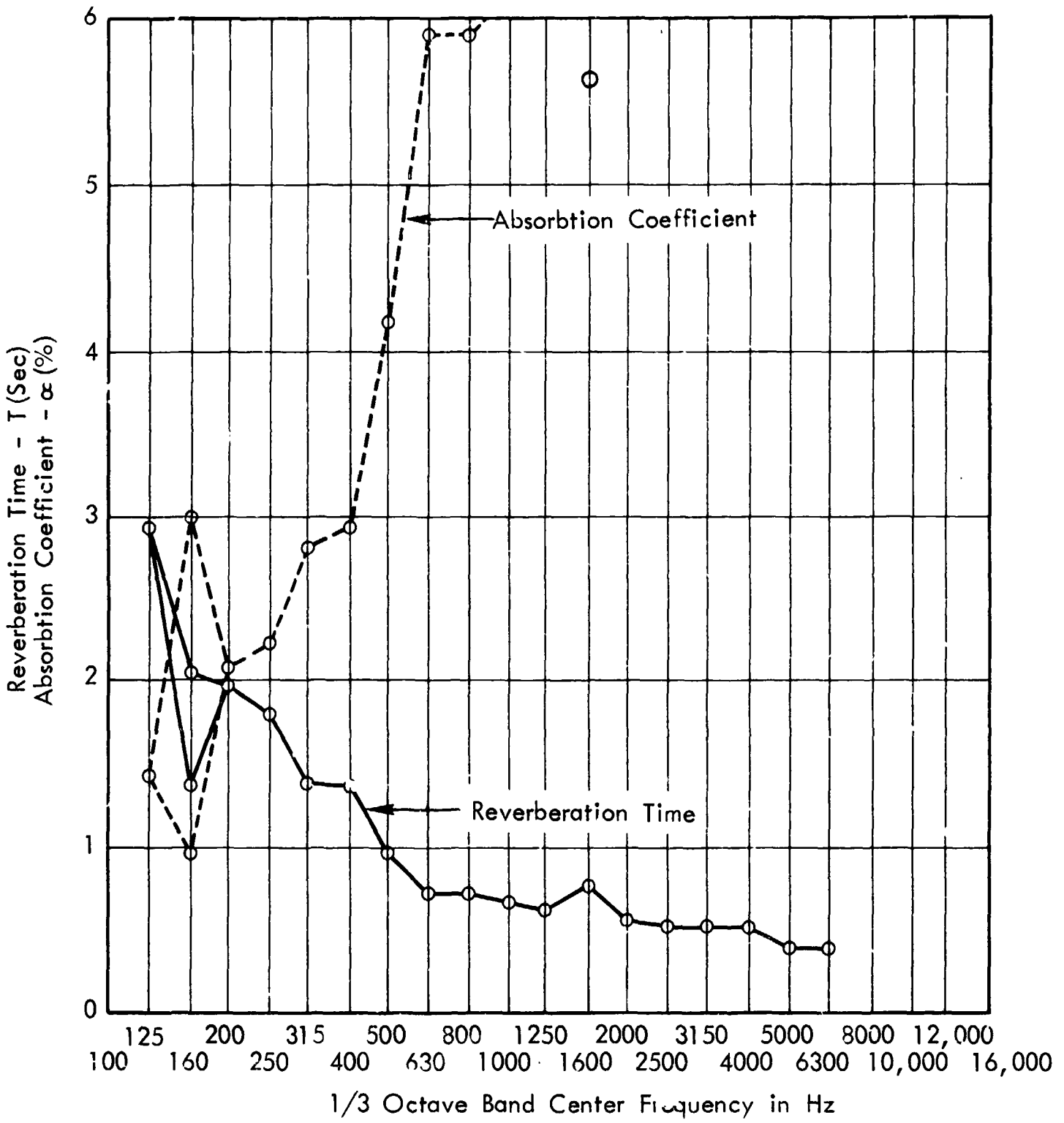

FIGURE 16. REVERBERATION TIME AND ABSORBTION COEFFICIENT OF RECTANGULAR CHAMBER WITH INCREASED ABSORBTION

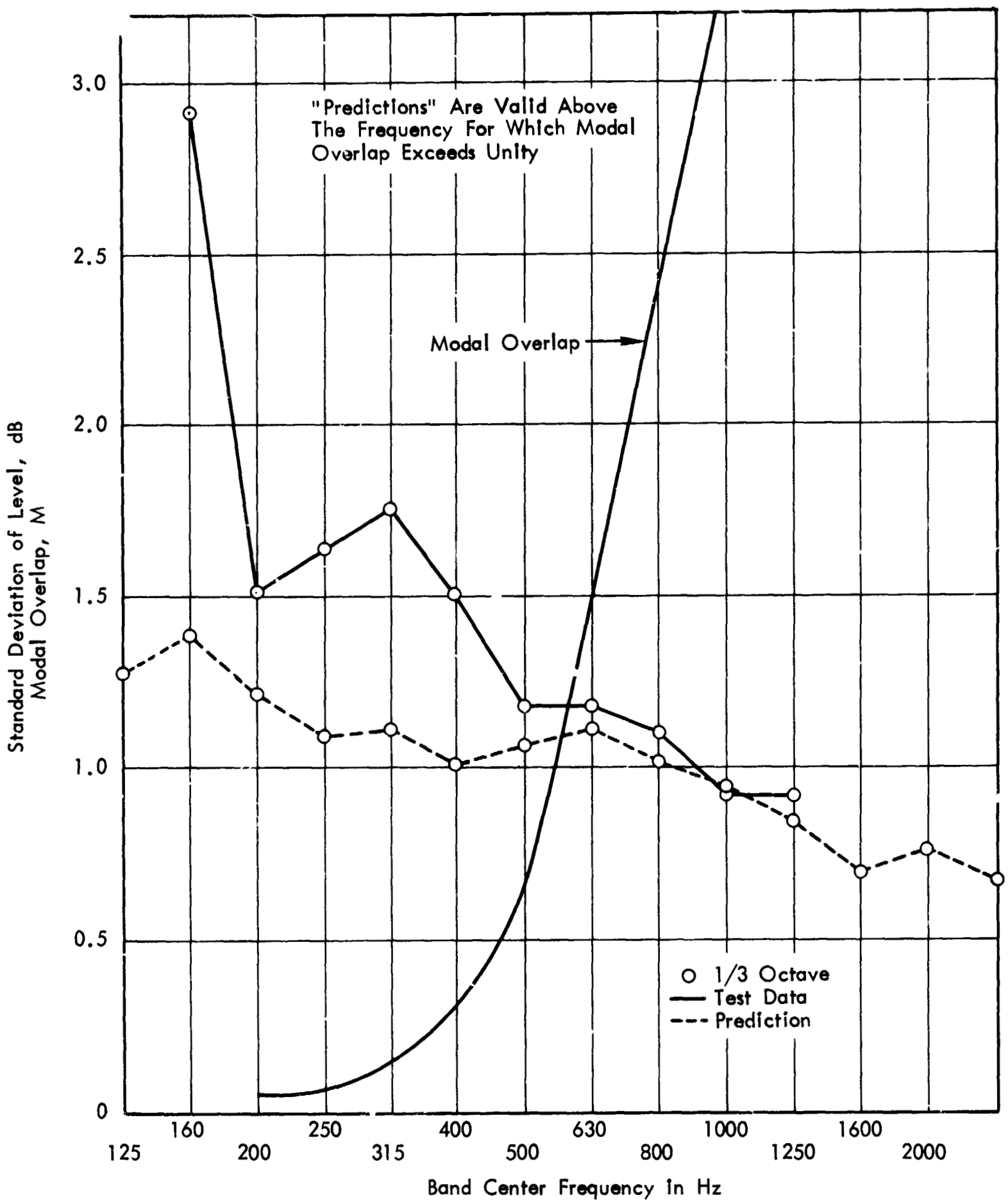

FIGURE 17. SPATIAL VARIATIONS IN RECTANGULAR CHAMBER WITH INCREASED ABSORBTION

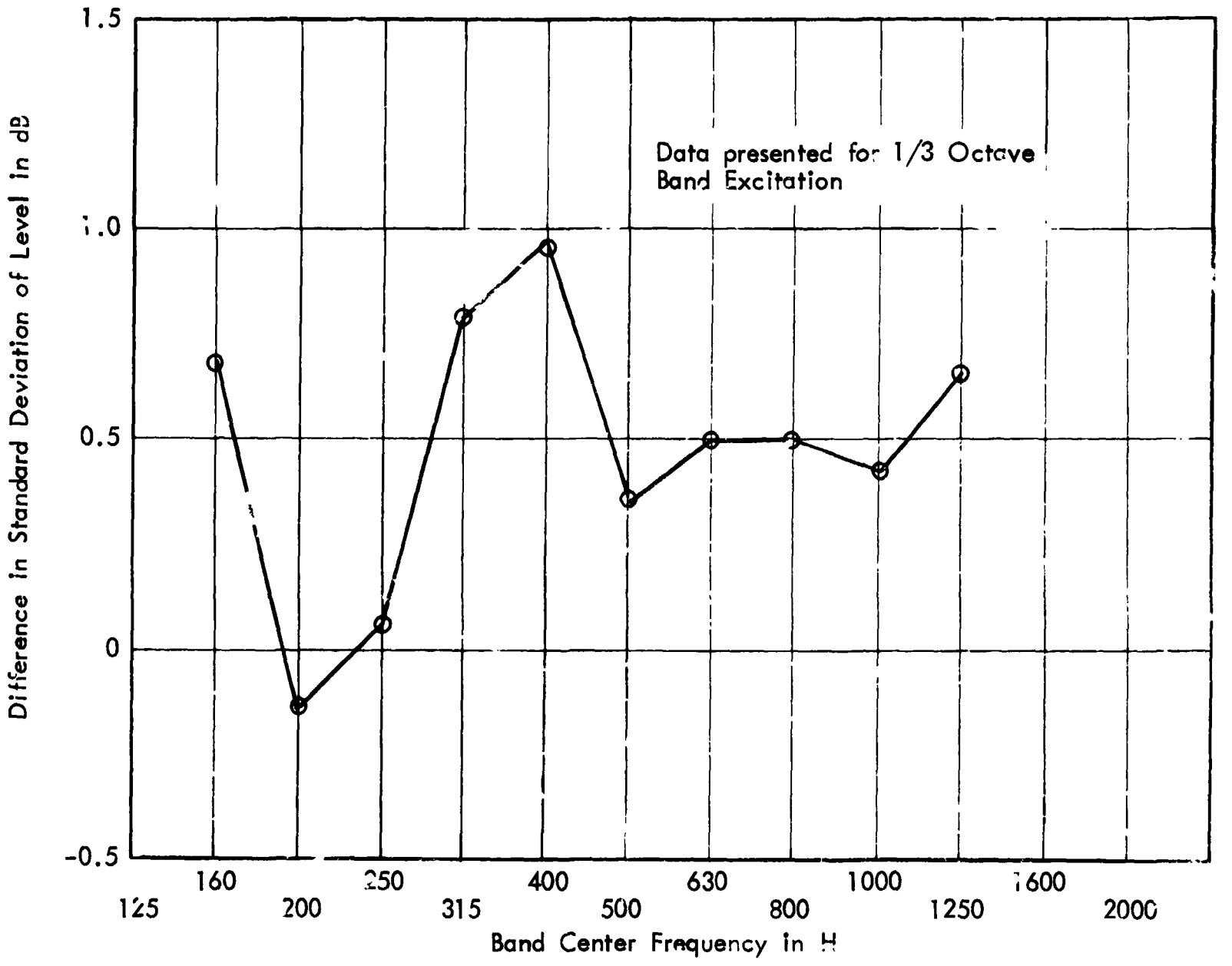

E 18. DIFFERENCE BETWEEN MEASURED SPATIAL STANDA[illegible]
[illegible]ATIONS WITH INCREASED ABSORB[illegible]ION AND WITH MOD[illegible]
ENRICHMEN[illegible] PANELS

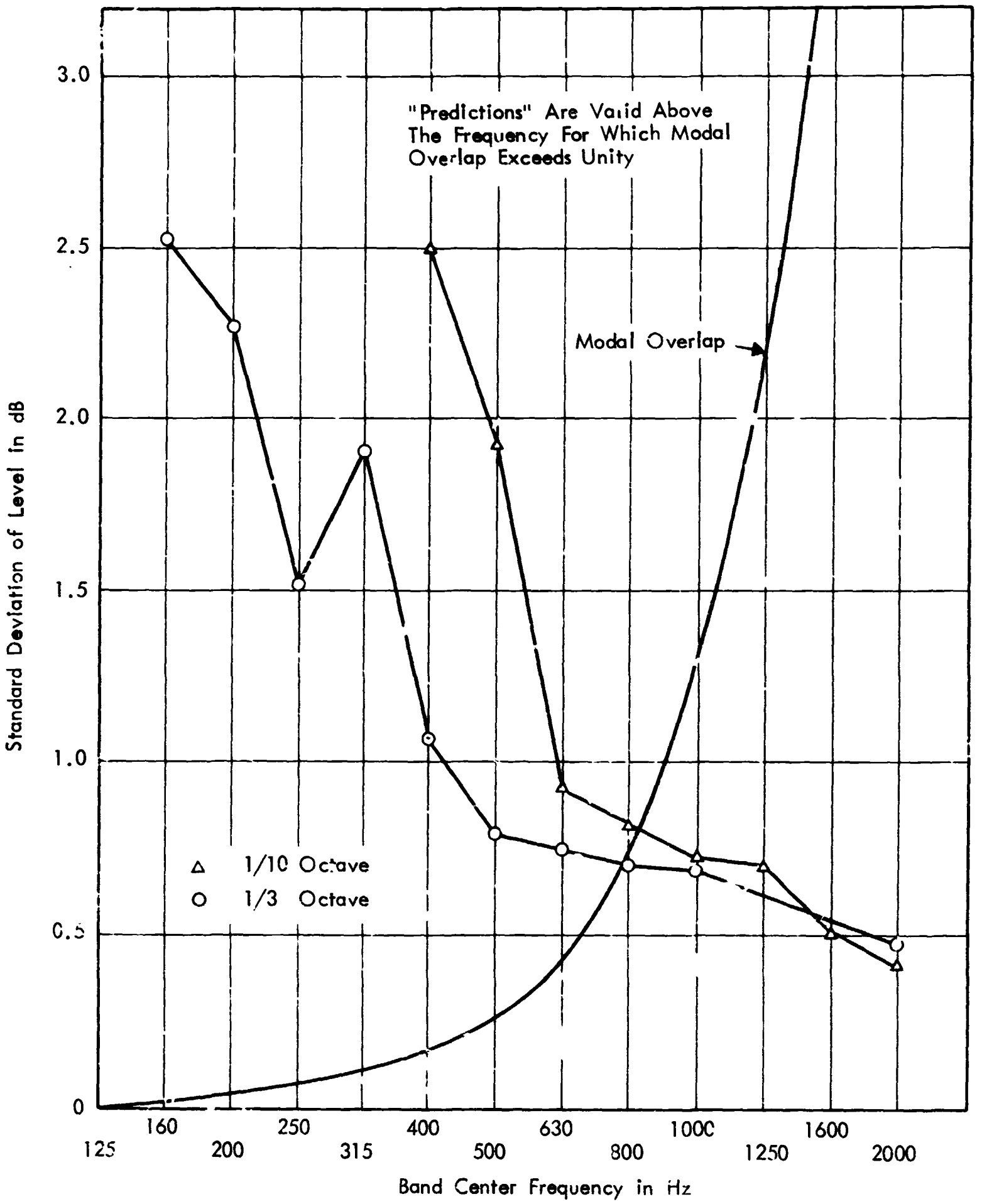

FIGURE 12. SPATIAL VARIATIONS IN RECTANGULAR CHAMBER EXCITED WITH TWO UNCORRELATED SPEAKER DRIVERS

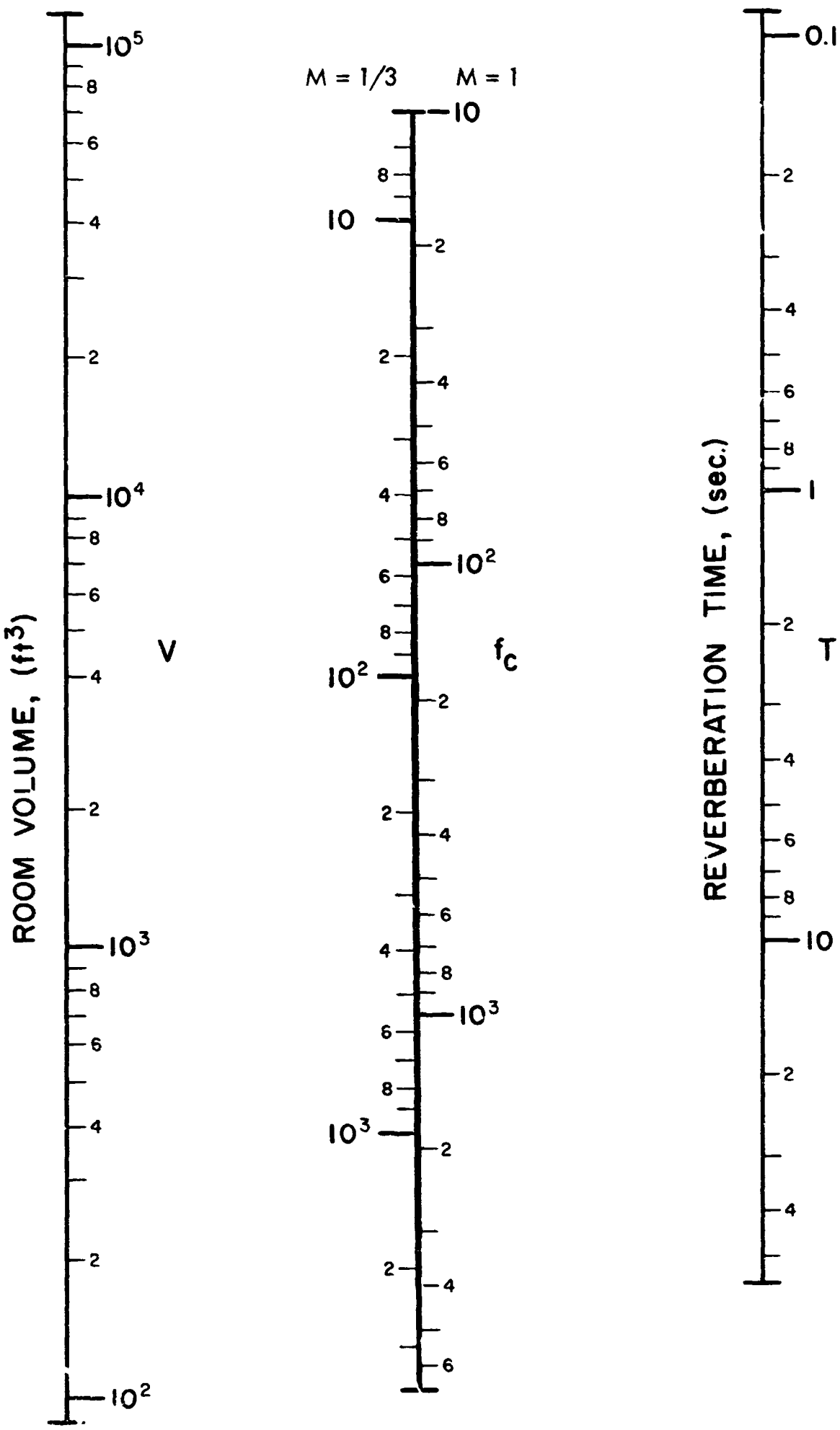

FIGURE 20. CUT-OFF FREQUENCY FOR GOOD STATISTICAL BEHAVIOR OF REVERBERANT ROOMS (EQ. 12)

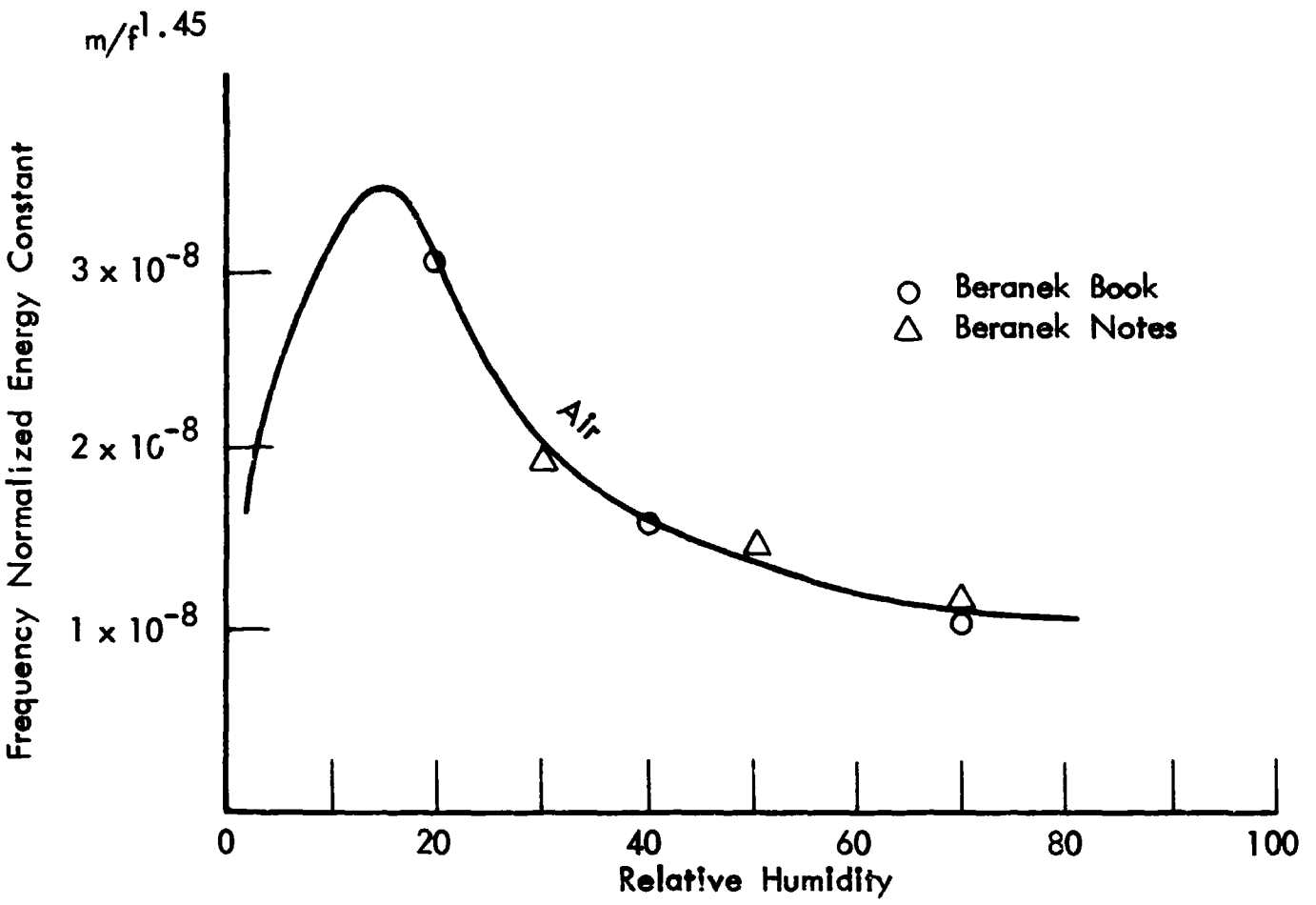

FIGURE 21. ENERGY ATTENUATION CONSTANT FOR AIR

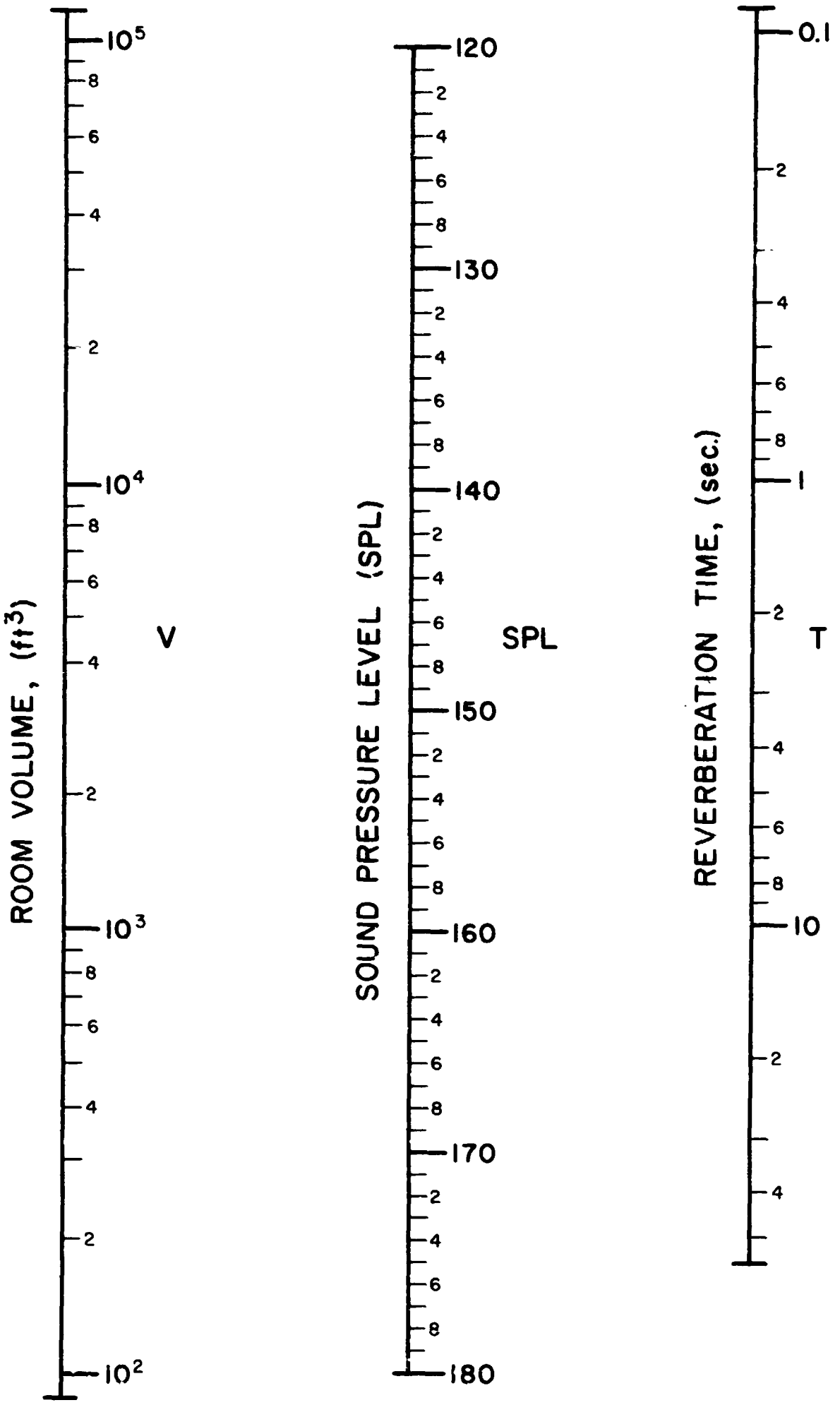

FIGURE 22. SOUND PRESSURE LEVEL FOR 1000 WATTS ACOUSTIC POWER INPUT (EQ. 14)

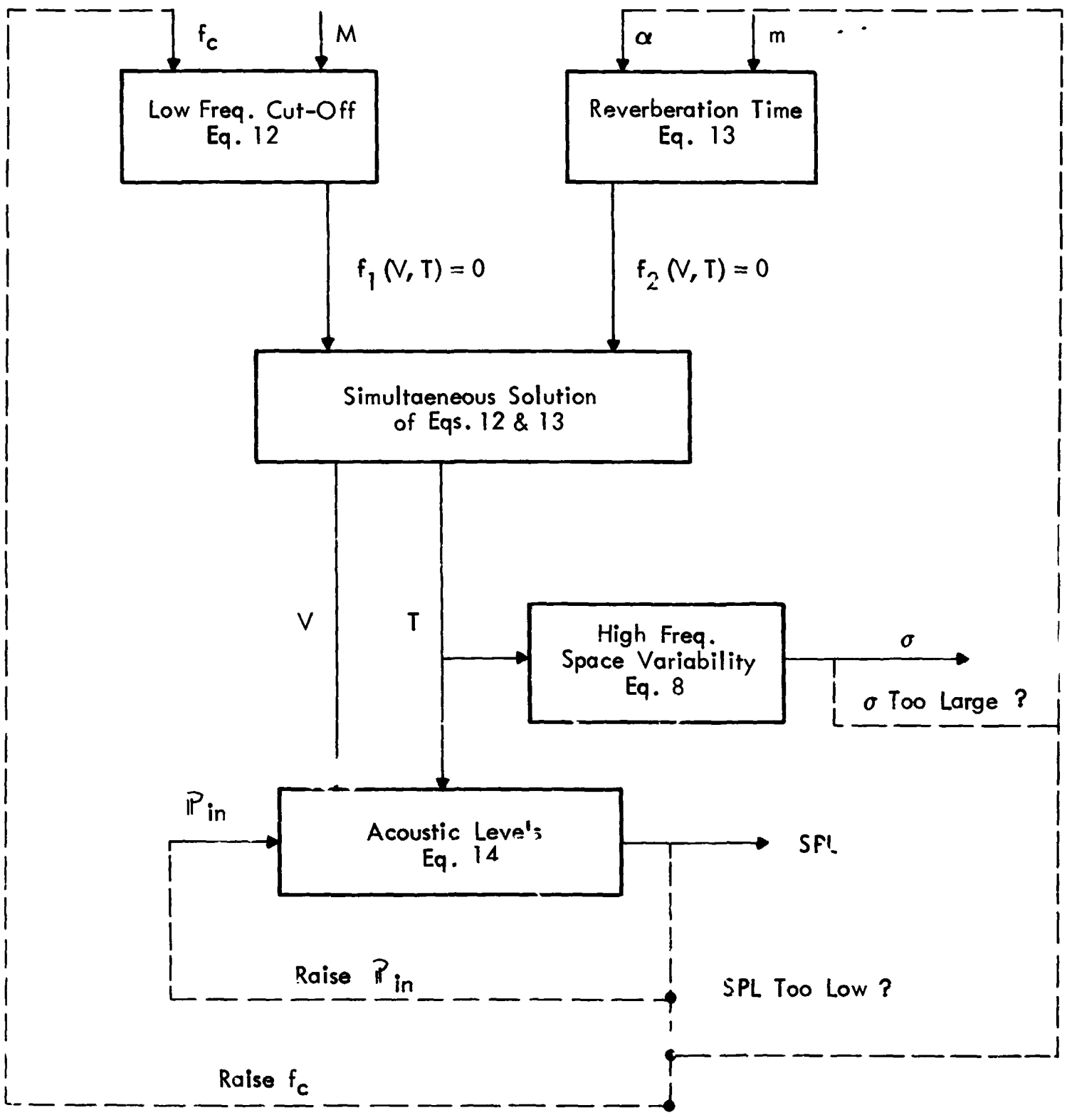

FIGURE 23. ITERATION PROCEDURE FOR REVERBERANT

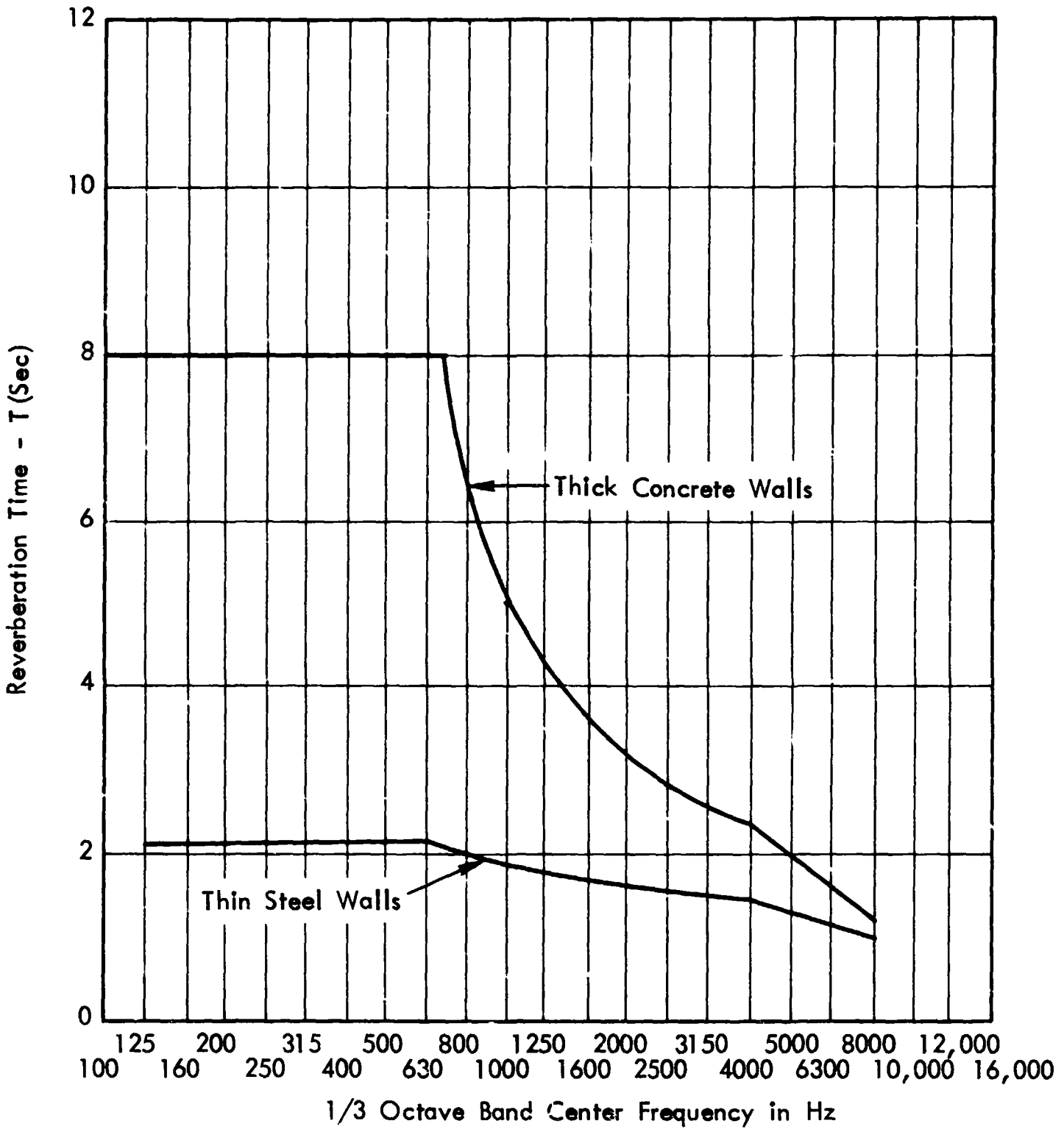

FIGURE 24. REVERBERATION TIME PREDICTION FOR GSFC 2135 CUBIC FOOT REVERBERATION CHAMBER

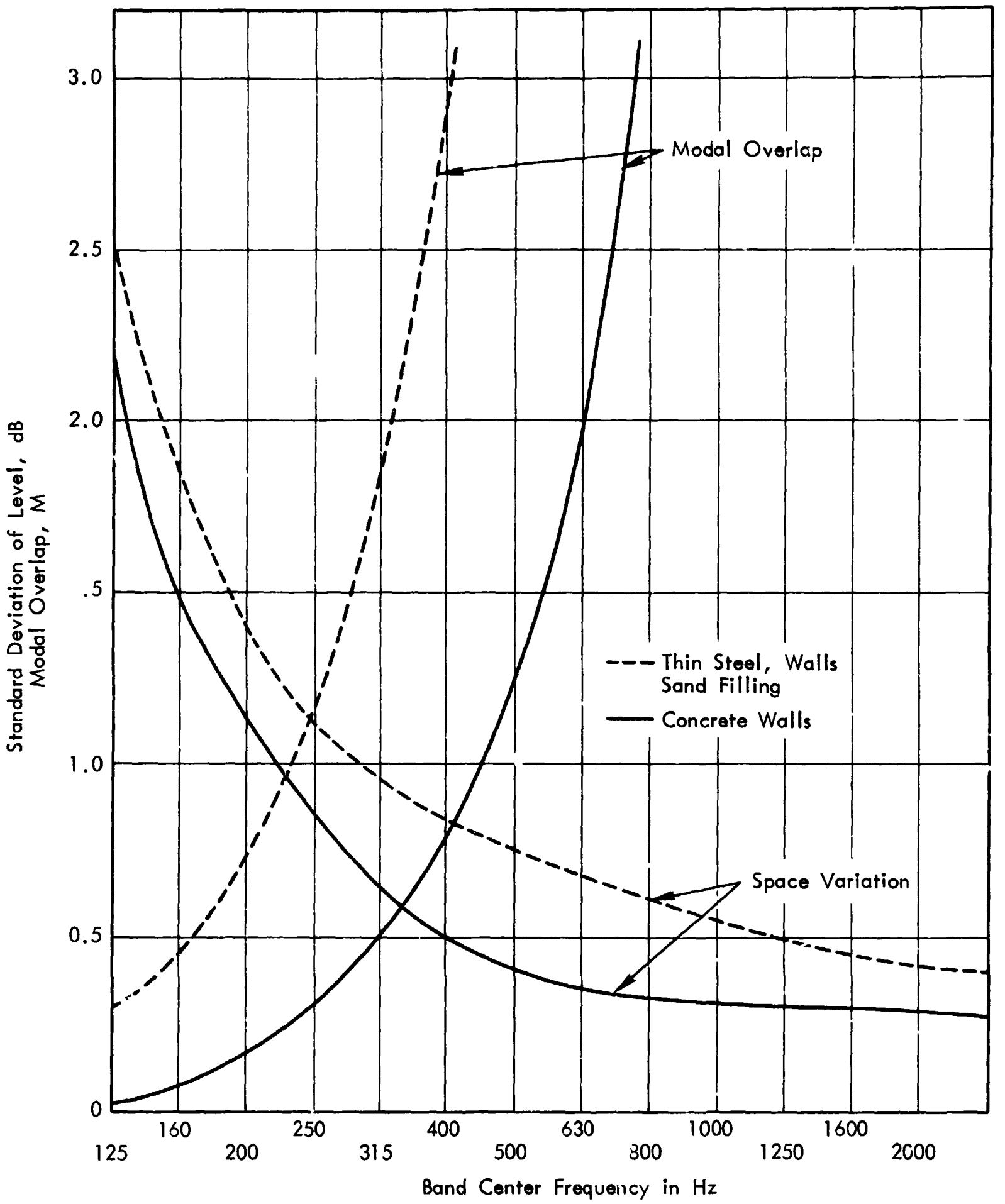

FIGURE 25. SPATIAL VARIATION PREDICTION FOR GSFC 2135 CUBIC FOOT REVERBERATION CHAMBER